Evaluating the Arabian Sea as a regional source of atmospheric CO$_2$: seasonal variability and drivers

Alain de Verneil[1], Zouhair Lachkar[1], Shafer Smith[2], and Marina Lévy[3]

[1]Center for Protoype Climate Modeling, New York University Abu Dhabi, Abu Dhabi, UAE
[2]Courant Institute of Mathematical Sciences, New York University, New York, USA
[3]Sorbonne Université (CNRS/IRD/MNHN), LOCEAN-IPSL, Paris, France

Correspondence: Alain de Verneil, (ajd11@nyu.edu)

Abstract. The Arabian Sea (AS) was confirmed to be a net emitter of CO$_2$ to the atmosphere during the international Joint Global Ocean Flux Study program of the 1990s, but since then little *in situ* data has been collected, leaving data-based methods to calculate air-sea exchange with fewer data and potentially out-of-date. Additionally, coarse-resolution models under-estimate CO$_2$ flux compared to other approaches. To address these shortcomings, we employ a high-resolution (1/24°) regional model

5 to quantify the seasonal cycle of air-sea CO$_2$ exchange in the AS by focusing on two main contributing factors, pCO$_2$ and winds. We compare the model to available *in situ* pCO$_2$ data and find that uncertainties in dissolved inorganic carbon (DIC) and total alkalinity (TA) lead to the greatest discrepancies. Nevertheless, the model is more successful than neural network approaches in replicating the large variability in summertime pCO$_2$ because it captures the AS's intense monsoon dynamics. In the seasonal pCO$_2$ cycle, temperature plays the major role in determining surface pCO$_2$, except where DIC delivery is

10 important in summer upwelling areas. Since seasonal temperature forcing is relatively uniform, pCO$_2$ differences between the AS's sub-regions are mostly caused by geographic DIC gradients. We find that primary productivity during both summer and winter monsoon blooms, but also generally, is insufficient to off-set the physical delivery of DIC to the surface, resulting in limited biological control of CO$_2$ release. The most intense air-sea CO$_2$ exchange occurs during the summer monsoon where outgassing rates reach $\sim$**6 molCm^{-2}yr^{-1}** in the upwelling regions of Oman and Somalia, but the entire AS contributes

15 CO$_2$ to the atmosphere. Despite a regional spring maximum of pCO$_2$ driven by surface heating, CO$_2$ exchange rates peak in summer due to winds, which account for $\sim$**90%** of the summer CO$_2$ flux variability versus **6%** for pCO$_2$ in a Reynolds decomposition. In comparison with other estimates, we find that the AS emits $\sim$**160TgCyr^{-1}**, slightly higher than previously reported. Altogether, there is **2x** variability in annual flux magnitude across methodologies considered. Future attempts to reduce the variability in estimates will likely require more *in situ* carbon data. Since summer monsoon winds are critical in

20 determining flux both directly and indirectly through temperature, DIC, TA, mixing, and primary production effects on pCO$_2$, studies looking to predict CO$_2$ emissions in the AS with ongoing climate change will need to correctly resolve their timing, strength, and upwelling dynamics.

1 Introduction

25 The global ocean represents a major reservoir of inorganic carbon on the planet's surface, and up to the present has on average acted to uptake excess anthropogenic CO_2 (Ciais et al., 2013; Khatiwala et al., 2009). The Arabian Sea (AS) is a region of the ocean that has been found to naturally release CO_2 to the atmosphere (Sarma et al., 1998), mitigating the ocean's role in moderating atmospheric CO_2 accumulation. While the AS as a regional basin is considered too small to greatly impact global budgets of air-sea CO_2 exchange (Naqvi et al., 2005), it attracts attention because some of the highest rates of air-sea CO_2 flux

30 and values of partial pressure of CO_2, or pCO_2, have been observed there, in addition to unique features such as the world's thickest oxygen minimum zone (OMZ) (Lachkar et al., 2016) and corresponding Carbon Maximum Zone (CMZ) (Paulmier et al., 2011).

The role of the AS as a region of net CO_2 emission, while suspected for decades (Keeling, 1968; Naqvi et al., 1993), was more firmly established with observations conducted under the international collaborative efforts of the Joint Global Ocean

35 Flux Study (JGOFS) program during the 1990s (Sarma et al., 1998; Millero et al., 1998a; Goyet et al., 1998b; Naqvi et al., 2005); see Smith (2005) and the accompanying Progress in Oceanography special issue for greater context. Conducted over several years, a major focus was to sample over the particularly strong seasonal monsoon cycle present in the AS, complete with surface current reversals, coastal upwelling, and intense phytoplankton blooms (Schott and McCreary Jr, 2001; Kumar et al., 2001; Lévy et al., 2007). JGOFS carbon data were first used to create linear statistical models, which were then extrapolated

40 over a greater region of the AS to produce larger-scale estimates of seasonal CO_2 flux showing emission to the atmosphere (Sabine et al., 2000; Sarma, 2003; Bates et al., 2006). JGOFS data still represent the greatest source of data for current de facto standard global products, such as Takahashi et al. (2009) (hereafter TK09), who produced a global climatology of pCO_2 and CO_2 flux gridded onto a 4° x 5° grid using a horizontal advection-diffusion scheme. In recent years, neural networks have been applied instead of simpler statistical models to likewise produce global climatologies, such as Landschützer et al. (2015)

45 (hereafter L15) on an increased-resolution 1° x 1° grid. All these different methodologies, although of differing sophistication, still rely on the availability of *in situ* data.

The wealth of information provided by the JGOFS expeditions has been invaluable for understanding the AS, but there has been little subsequent *in situ* sampling in the AS, as has been previously remarked (Hood et al., 2016). For example, in the Global Ocean Data Analysis Project v2 (GLODAP; Olsen et al., 2019) database, there are no reported observations in the AS

50 of two important carbon variables, dissolved inorganic carbon (DIC) and total alkalinity (TA), more recent than 1998, with a similar story for pCO_2. Thus, the global products of TK09 and L15 are based upon conditions in the AS from 20 years ago. Since quantities like surface pCO_2 concurrently trend with rising atmospheric CO_2 concentration (Tjiputra et al., 2014), the dearth of recent sampling means that uncertainty in the AS's carbon system will only grow with time. The gap in data collection also means that the AS is proportionally under-represented in global datasets: whereas the AS is 2% of the ocean surface, DIC

55 and TA measurements in the AS are <1% of the GLODAP ensemble, which is also the case with pCO_2 reported in the Surface Ocean Carbon ATlas (SOCAT; Bakker et al., 2016; Pfeil et al., 2013).

Where data are sparse in the AS, numerical circulation models have been used to complement the lack of spatiotemporal coverage. These models fill the domain with their own estimates of carbon variables, such as pCO_2, while also providing detailed information on the factors affecting them, e.g. DIC, temperature, biological productivity, etc. For example, in the

60 wake of the JGOFS expeditions, the synthesis study of Sarma et al. (2003) used a numerical model to examine biological and chemical aspects of the annual carbon budget in the central and eastern AS. Further studies focus on other aspects over different timescales, such as intraseasonal pCO_2 variability due to temperature versus DIC (Valsala and Murtugudde, 2015), or decadal trends in pH (Sreeush et al., 2019a). These approaches, without more *in situ* data, are the best estimates we have of the current AS carbon system's behavior. Therefore, it is incumbent that these models are vigorously validated against

65 what precious few data exist. The need is further emphasized when quantities such as pCO_2 can be utilized as a proxy for other things, such as community compensation depth (Sreeush et al., 2019b). However, most recent studies compare output to established climatologies, such as TK09, which are coarse in spatial resolution and smooth out unique features of the AS such as coastal upwelling, although some studies have begun using ARGO float profiles for model validation (Chakraborty et al., 2018).

70 Despite the wealth of information that models provide, they have their own weaknesses. In a review of CO_2 flux estimates from various independent methodologies, Sarma et al. (2013) found that coupled ocean biogeochemical models underestimated the air-sea CO_2 flux. The underestimate was attributed to poor resolution of monsoonal currents, specifically near the coasts of Oman and Somalia. The need for sufficient resolution of monsoon and upwelling currents is underscored by the roles that small-scale horizontal (Mahadevan et al., 2004) and vertical (Mahadevan et al., 2011; Resplandy et al., 2019) currents can

75 play in advecting carbon. Additionally, Sarma et al. (2013) found that the peak of flux observed in boreal summer occurred slightly out of phase, with models leading observations by over a month in the AS. Finally, the modeled pCO_2 in the AS found a springtime maximum not seen in the observations based on the data from TK09. Clearly, an effort must be made to establish whether these discrepancies are residual effects of low resolution, endemic to models generally, or indicative of a real pattern that suggests future concerted *in situ* sampling.

80 Considering the challenges specific to studying the AS carbon cycle, in this paper we aim to put into context the role of the AS as a CO_2 source by quantifying air-sea CO_2 flux with a targeted approach. First, by employing a higher-resolution regional numerical model of the AS carbon system, monsoonal and upwelling currents will be sufficiently resolved. Furthermore, model validation will use raw data, not a smoothed climatological product, to evaluate the model. Quantification of air-sea flux will focus on the contributing factors of pCO_2 and wind. In particular, the role of temperature (T), salinity (S), DIC, and TA in

85 determining the seasonal cycle of pCO_2 will be investigated, which of course also varies from region to region within the AS. A further budget analysis of surface DIC compares the physical and biological mechanisms governing carbon sources and sinks, such as advection and mixing versus biological production and respiration. The relative impact of pCO_2 and winds upon the seasonal cycle of CO_2 flux are also compared, culminating in a meta-analysis of the model's CO_2 flux estimates relative to alternative approaches.

90 For this study, we choose to focus on the seasonal cycle due to the strength of the monsoon in the AS and because it is resolved by the data, although interannual (Valsala and Maksyutov, 2013; Valsala et al., 2020) and intraseasonal (Valsala and

Murtugudde, 2015) variability exists. The rest of the paper will start with a description of pCO$_2$ datasets used, along with the model configuration and methods of analysis in Section 2. Following this in Section 3 is a description of the model validation and results, with discussion in Section 4. We conclude in Section 5 with perspectives and recommendations regarding future

95 studies of pCO$_2$ and air-sea CO$_2$ flux in the AS.

2 Methods

2.1 pCO$_2$ data

In this study, pCO$_2$ is used as the primary *in situ* data for model validation. Whereas models favor DIC and TA (Wolf-Gladrow et al., 2007), shipboard pCO$_2$ can be measured underway and hence there are more observations available. Additionally, since

100 model pCO$_2$ is calculated from DIC and TA, pCO$_2$ measurements act as an independent dataset. Here, pCO$_2$ validation stems from *in situ* un-gridded data merged from SOCAT v. 2019 (downloaded from https://www.socat.info/index.php/version-2019/ September 2019) and the Lamont-Doherty Earth Observatory (LDEO) surface pCO$_2$ database (Takahashi et al., 2019). Due to the large overlap in the two databases, SOCAT data was preferred to LDEO observations, and LDEO observations were included for years where SOCAT data are unreported. SOCAT fugacity (fCO$_2$) values were converted to pCO$_2$ and mole

105 fraction (xCO$_2$) using reported sea surface temperature (SST) and S data included in the products. The anthropogenic effect of increasing surface pCO$_2$ was calculated by removing a fit linear trend of 2 µatm yr^{-1}, slightly higher than ≈1.5 seen in Tjiputra et al. (2014). pCO$_2$ values were calibrated to the year 2005, the representative year used for the model's atmospheric xCO$_2$.

Alternative pCO$_2$ products are used for comparison purposes. The gridded products from TK09 and L15, while based

110 upon the same *in situ* data mentioned above, represent different processing methodologies. pCO$_2$ is also calculated from DIC and TA provided by the statistical fits to JGOFS data by Sarma (2003) and to the gridded GLODAP climatological product. The statistical fits of Sarma (2003) were used twice, first using model T,S, and Chl-*a*, and second with World Ocean Atlas (WOA) 2009 T, S with SeaWifs Chl-*a*. GLODAP-derived pCO$_2$ also uses WOA2009 T, S. Calculations of pCO$_2$ are performed using the CO2SYS software package (Van Heuven et al., 2011). Since all calculations are conducted at the near-

115 surface, differences between this software suite and Orr and Epitalon (2015) are minimal. For air-sea flux calculations, all ΔpCO$_2$ values were calculated using Keeling curve values (downloaded from https://www.esrl.noaa.gov/gmd/ccgg/trends/gl_data.html, downloaded September 2019) of atmospheric xCO$_2$ for the respective calibrated year of each data set (1995 for Sarma (2003), 2001 for L15, 2002 for GLODAP, 2005 for TK09). A summary of these datasets and their characteristics is provided in Table 1.

120 ### 2.2 Model details and set-up

The model we use is the Regional Ocean Modeling System-AGRIF (ROMS-AGRIF) 3.1.1. Shchepetkin and McWilliams (2005). Previously used in the region (Lachkar et al., 2016), the model is a free-surface primitive equation model, with a sigma

and curvilinear grid for the vertical and horizontal dimensions, respectively. ROMS implements a forward-backward time-stepping alogrithm with split baroclinic and barotropic modes. The advection of tracers implements a rotated-split 3rd order
125 upstream biased algorithm for the advection of tracers to reduce spurious mixing (Marchesiello et al., 2009). The K-profile parameterization (KPP; Large et al., 1994) for vertical mixing is used. The model domain spans from 5.3^{o}S to 30.5^{o}N, and from 33° to 78.1^{o}E (Fig. 1). For the sake of comparison with previous studies, we will present the region north of the equator, and exclude the Red Sea and Arabian Gulf. The model's horizontal resolution is $1/24^{o}$, resulting in $\sim$5km horizontal grid spacing.

130 Coupled to the hydrodynamic model is a nitrogen-based biogeochemical model with two components for nutrients, nitrate and ammonium, with one phytoplankton, zooplankton, and two detrital pools (Gruber et al., 2006). Biological parameters for the model are the same as those used in Gruber et al. (2011). A carbon module is also applied to the model with the state variables of DIC, TA, and calcium carbonate ($CaCO_3$) (Gruber et al., 2012; Hauri et al., 2013; Lachkar and Gruber, 2013). In addition to usual physical transport and mixing, $CaCO_3$ is allowed to vertically sink at 20 $mday^{-1}$. Organic car-
135 bon is linked to organic nitrogen through the Redfield ratio 106:16. DIC is altered by air-sea CO_2 flux, primary production, respiration/remineralization, and dissolution/precipitation of $CaCO_3$. TA changes with the removal and creation of nitrate (NO_3) as well as dissolution/precipitation of $CaCO_3$. The amount of $CaCO_3$ precipitation is linked to primary production through a constant ratio of 0.07, meaning 0.07 moles of $CaCO_3$ are produced for each mole of organic carbon. The dissolution rate is a constant 0.0057 day^{-1} in the water column and 0.002 day^{-1} in the sediments. Surface fluxes of DIC and
140 TA due to evaporation and precipitation were included as virtual fluxes. Inside the module, surface carbon chemistry is calculated using routines from the Ocean Carbon-Cycle Model Intercomparison Project (OCMIP) carbonate chemistry routines (http://ocmip5.ipsl.jussieu.fr/OCMIP/phase3/simulations/). Carbon chemistry coefficients used here include K_1 and K_2 CO_2 dissociation from Millero (1995), original data from Mehrbach et al. (1973) and refit by Dickson and Millero (1987).

The model was run in climatological mode, with 360-day years and interpolated monthly forcing. Heat flux, evaporation and
145 precipitation, and surface salinity were provided by the Comprehensive Ocean-Atmosphere Data Set (COADS; da Silva et al., 1994). SST forcing is provided by a monthly climatology of Pathfinder data from 1985-1997 (Casey and Cornillon, 1999). Wind stress was produced using the QuikSCAT/SCOW monthly climatology from 1999-2009 (Risien and Chelton, 2008). Tracer values for the initial conditions and the boundaries are given by WOA 2009 for T, S, NO_3, and oxygen. Horizontal velocities u,v for initial and boundary conditions derive from the Simple Ocean Data Assimilation (SODA) analysis (Carton
150 and Giese, 2008). Initial and boundary conditions for DIC and TA come from GLODAP from 300m down to the bottom. Surface TA was calculated using the relations from Lee et al. (2006), and the corresponding DIC was calculated using WOA phosphate, silicate, T, and S values along with L15 pCO_2. DIC and TA values between the surface and 300m were calculated using density-weighting. The model was spun up for 30 years, with 5 additional years for analysis. Atmospheric xCO_2 values are set to 380ppm, equivalent to 2005 levels, with an annual sinusoidal perturbation of 2.9ppm.

2.3 Domains of Analysis

In this study we focus on 6 distinct regions (Fig. 1). The first, the entire analysis domain, is the AS north of the equator. The upwelling regions of the Oman and Somalian coasts are included separately to focus on the summer monsoon impact of enhanced DIC but also enhanced biological productivity. The Oman region begins at the coast and extends 300km outward. The Somalia region begins near 3.8^oN and extends north to the tip of the Horn of Africa, with an eastern extension to 58.6^oE so as to encompass the region known as the Great Whirl (Vic et al., 2014), shown to be important for air-sea exchange in previous studies (Valsala and Murtugudde, 2015). The North region is defined by a rectangle from 59.4^oE, 21^oN to 69.5^oE, 26.5^oN, encompassing the northern part of the AS where the winter monsoon's primary productivity is most intense. An oligotrophic region representing the central AS, which has less productivity and chlorophyll-a on average (Fig. 1), is defined by a rectangle from 61.31^oE, 3.3^oN to 70.8^oE, 17^oN. The last region, covering the western coast of India, extends from the coastline 100km offshore.

2.4 Analysis of pCO$_2$, DIC, and air-sea CO$_2$ flux variability

2.4.1 pCO$_2$ variability

The proximate variables impacting pCO$_2$ in the model are DIC, TA, T, and S. Following previous studies (Lovenduski et al., 2007; Turi et al., 2014), we use a first-order Taylor expansion to decompose pCO$_2$ into contributions from these four, neglecting contributions from nutrients (phosphate and silicate). Initially, the decomposition would follow the form

$$\Delta pCO_2 \approx \frac{\partial pCO_2}{\partial DIC}\Delta DIC + \frac{\partial pCO_2}{\partial TA}\Delta TA + \frac{\partial pCO_2}{\partial T}\Delta T + \frac{\partial pCO_2}{\partial S}\Delta S \qquad (1)$$

where ΔpCO$_2$ is the perturbation of pCO$_2$ from a mean value, and the Δ terms for DIC, TA, T, and S likewise express deviations from an average. However, in order to control for salinity effects on DIC and TA (Keeling et al., 2004), we normalize DIC and TA by the salinity $S_0=35$ psu, to create the variables

$$DIC^s = S_0\frac{DIC}{S} \ \ and \ \ TA^s = S_0\frac{TA}{S}. \qquad (2)$$

Substituting these terms into Eqn. (1), we can expand to produce, for example with DIC, the following (Lovenduski et al., 2007):

$$\frac{\partial pCO_2}{\partial DIC}\Delta DIC = \frac{\partial pCO_2}{\partial(S/S_0 DIC^s)}\Delta(S/S_0 DIC^s)$$
$$= \frac{DIC^s}{S_0}\frac{\partial pCO_2}{\partial DIC}\Delta S + \frac{S}{S_0}\frac{pCO_2}{\partial DIC}\Delta DIC^s. \qquad (3)$$

Collectively, the ΔS term in Eqn. (3) and its counterpart in TA can be added to the original ΔS term in Eqn. (1) to represent all salinity effects in a "freshwater" term, FW, so that we now have (Turi et al., 2014)

$$\Delta pCO_2 \approx \underbrace{\frac{\partial pCO_2}{\partial DIC^S}\Delta DIC^S}_{\Delta pCO_2^{DIC^s}} + \underbrace{\frac{\partial pCO_2}{\partial TA^S}\Delta TA^S}_{\Delta pCO_2^{TA^s}} + \underbrace{\frac{\partial pCO_2}{\partial T}\Delta T}_{\Delta pCO_2^{T}} + \underbrace{\frac{\partial pCO_2}{\partial FW}\Delta FW}_{\Delta pCO_2^{FW}}. \qquad (4)$$

For the remainder of this paper, when discussing the results of the Taylor series decomposition method, it will be understood that DIC and TA refer to DIC^s and TA^s.

The contributions of DIC, TA, T, and S to pCO_2 variability are used to construct maps and timeseries of pCO_2 anomalies.
185 In order to calculate the anomaly ΔpCO_2 requires calculating both the Δ deviations of DIC, TA, T, and FW, as well as partial derivatives. In this study, we calculate both temporal and spatial anomalies. To consider spatial variability, starting with annual means of pCO_2, DIC, TA, T, and S, an average value for the whole domain is calculated and removed from each grid point's annual mean to get a Δ perturbation, or anomaly. Similarly, for temporal variability, with the monthly values of pCO_2, DIC, TA, T, and S at each grid point, the annual average at that grid point is removed to produce the monthly Δ perturbation/anomaly.
190 Partial derivatives are approximated via centered differences. These are obtained by calculating pCO_2 with slight deviations of DIC, TA, T, and S from the mean value. Both positive and negative deviations are used to construct centered differences, with deviation magnitude determined by Orr et al. (2018).

2.4.2 DIC budget

Whereas the state variables of DIC, TA, T, and S provide the chemical context which determines carbon availability to potential
195 air-sea flux via pCO_2, tracking the overall inventory of inorganic carbon (i.e. DIC), allows for the parsing of numerous source and sink processes governing the total amount of carbon reaching the surface. Beyond the biological processes impacting DIC as outlined in Sect. 2.2, the physical processes impacting DIC are air-sea CO_2 flux, surface evaporation and precipitation, horizontal and vertical advection, and horizontal and vertical mixing. In order to diagnose the relative importance of these terms (i.e. to weigh competition between upwelling circulation-source and biological drawdown-sink), we calculate the budget
200 I_{DIC} in a 3D volume by integrating:

$$I_{DIC} = \iint_{\mathbf{A}} \int_{-z(\sigma)}^{\eta} J(x,y,z) \, d\mathbf{A} \, dz \tag{5}$$

with

$$J = \underbrace{-PP_{New+Reg} - CaCO_{3prec-remin} + Zoo_{resp} + Det_{remin}}_{NPP-Remin\,(Biology)} - \underbrace{F_{AS}}_{Air-Sea}$$
$$+ \underbrace{Adv_x + Adv_y + Mix_x + Mix_y}_{Horz.\,Circ} + \underbrace{Adv_z + Mix_z}_{Vert.\,Circ} + \underbrace{Evap - Precip}_{Forc}, \tag{6}$$

which is the volume-specific flux J of DIC in a given grid cell. $PP_{New+Reg}$ is net community primary production scaled by
205 the Redfield ratio, $CaCO_{3remin-prec}$ is net $CaCO_3$ precipitation and remineralization, Zoo_{resp} is zooplankton respiration, and Det_{remin} is remineralization of both detrital pools. All these terms are grouped together into $NPP - Remin$ because they represent all biological processes. F_{AS} is air-sea flux, with a sign convention of positive outward. Adv_x is advective flux in the x-direction, with corresponding y and z components. Mix_x is the x-component of mixing flux, again with y and z components. All x and y components of both advective and mixing DIC fluxes are grouped into horizontal circulation, with
210 a similar grouping for vertical circulation in the z-direction. $Evap - Precip$ is the forced virtual flux from evaporation and

precipitation at the surface. $\mathbf{A}$ is the two-dimensional horizontal area to be considered, which in our study includes the entire domain but also the sub-regions of analysis. The bottom boundary of integration, $-z(\sigma)$, is the sigma-layer depth at which integration starts, moving up to the free-moving surface η. We chose to integrate the top five sigma layers of the model, corresponding to ~20m depth. This level was chosen because below this depth, annual cycles of I_{DIC} begin to deviate from

215   the surface DIC, which is our focus in this study of air-sea CO_2 flux.

2.4.3   Air-sea CO_2 variability

The air-sea flux in the model is calculated using

$$F_{CO_2} = K_0\,\alpha\,(pCO_2^{sea} - pCO_2^{air})$$
$$= K_0\,\alpha\,\Delta pCO_2 \tag{7}$$

where K_0 is the solubility determined by temperature and salinity (Weiss, 1974), α is the CO_2 piston velocity with a quadratic

220   wind speed dependence (Wanninkhof, 1992), and the difference in ocean and atmosphere pCO_2, ΔpCO_2, is arranged so that the flux convention is positive outward from the ocean. The objective being to characterize seasonal anomalies of air-sea CO_2 flux, here we use a Reynolds decomposition (Doney et al., 2009). Noting that temperature effects upon solubility (K_0) and piston velocity (α) approximately cancel, meaning that their product mostly reflects wind forcing, we have the following arrangement for the decomposition of flux anomalies (see Doney et al. (2009) for the derivation):

225    $$F'_{CO_2} = \underbrace{(K_0\,\alpha)'\overline{\Delta pCO_2}}_{\text{wind}} + \underbrace{\overline{(K_0\,\alpha)}\Delta pCO_2'}_{\text{pCO}_2} + \underbrace{\left((K_0\,\alpha)'(\Delta pCO_2)' - \overline{(K_0\,\alpha)'\Delta pCO_2'}\right)}_{\text{cross terms}}, \tag{8}$$

where $'$ indicates an anomaly and $\overline{x}$ is a five-year average of variable x, which are calculated at each grid point. F'_{CO_2} is the seasonal flux anomaly, with groupings based on wind anomalies $(K_0\,\alpha)'$, $\Delta pCO_2'$ anomalies, and cross-terms involving both.

3   Results

3.1   Model validation and pCO$_2$ data-model comparisons

230   The implementation of ROMS-AGRIF presented here has been used in previous studies (Lachkar et al., 2016). Model output of net primary productivity (NPP) captures the summer monsoon highs near the upwelling regions of Oman and Somalia, with enhanced NPP in the North during the winter monsoon (Fig. 1). The model also reproduces well the distribution of temperature, salinity, and surface velocities in comparison with established climatologies (Fig. S1-S3).

Regarding pCO_2, *in situ* data from the merged SOCAT/LDEO database shows that average binned ΔpCO_2 values in the

235   region are positive for most of the AS (Fig. 2a). The ensemble of observations show that $\sim90\%$ of ΔpCO_2 observations are positive, indicating positive flux to the atmosphere (Fig. 2a, inset). The monthly distribution of pCO_2 sampling (Fig. 2b) also shows that the majority of data ($\sim70\%$) come from the summer monsoon months (June-September JJAS), and that most observations date from the 1990s, with 96% coming from the years 1995 and 1997 alone.

Seasonal pCO_2 distributions from both data and the model are shown in Fig. 3. During the winter monsoon, pCO_2 values are
240 at their lowest (348-455 µatm; Fig. 3a). Spring intermonsoon (Fig. 3b) finds pCO_2 values similar to the winter (354-451 µatm),
with data coverage improving in the western AS. Summer monsoon, with best data coverage (Fig. 3c), has pCO_2 peaking at
773 µatm. In contrast, the fall intermonsoon (Fig. 3d) has very little data coverage (311-485 µatm). Similar to the data, model
pCO_2 (Fig. 3e) is at its lowest during the winter, but in the spring, open-ocean pCO_2 finds its peak, which is not reflected in
the *in situ* data set (Fig. 3b,f). Maximum model pCO_2 is found in the summer monsoon near upwelling reigons (Fig. 3g). Fall
245 model pCO_2 still has elevated values, but less than the summer period. Certain regions in the model show persistent maxima
in pCO_2, such as the Gulf of Oman and the Strait of Hormuz, which are not reflected in the few data collected there. Similarly,
model pCO_2 values in the Gulf of Aden increase during spring and then peak during the summer, a pattern which is unclear
from the data.

A Taylor diagram (Taylor, 2001) comparing *in situ* pCO_2 data and model output shows the relative performance of the model
250 (Fig. 4). For the entire dataset, as well as for the spring and summer seasons, the model's correlation with data is ∼0.5. Winter
and fall have lower values at 0.2 and 0.06, respectively. Variability expressed as normalized standard deviation shows that
overall, and during spring and summer periods, the model under-estimates data variability, but over-estimates it during winter
and fall. For all periods apart from summer, model pCO_2 has a positive bias (2.1, 24.6, 48.4, and 33.7 µatm for the annual,
winter, spring, and fall seasons, respectively). During the summer, the model has a negative bias of -3.1 µatm.

255 Since the model successfully replicates other tracers, physics, and biological processes (Fig. 1, Fig. S1-S3), we look for
the source of bias within the four state variables T, S, DIC, and TA in comparison with data. T and S from the merged
LDEO/SOCAT database, and DIC, TA, from the ungridded GLODAP product are compared with model output (Fig. S4). In
this case, model SST and surface salinity (Fig. S4a,b) largely overlap with a 1:1 relationship, but with slight positive biases
of ≈0.4°C and 0.3psu. Removing these biases from the model results in a pCO_2 shift of -6.8 and -3.5 µatm for T and S,
260 respectively, close to reported measurement error. Ungridded DIC and TA data from GLODAP, though more sparse (n=334
data points with both DIC and TA at depth ≤ 50m), show more deviation from the 1:1 line (Fig. S4c,d) with overall negative
biases of -15.8 µmolkg^{-1} and -30.0 µmol − eqkg^{-1} for DIC and TA. These biases result in pCO_2 perturbations of -33.8 and
+45.7 µatm, respectively, when accounted for individually. Since the buffering capacity of seawater is related to the ratio of
TA and DIC, when both biases are considered average pCO_2 shifts +16.7 µatm. As a result, while the DIC model bias lowers
265 pCO_2, the stronger bias in TA is the most likely cause for the model's overall positive pCO_2 bias.

Comparisons between the monthly probability distribution functions of pCO_2 from *in situ* data, model output, and L15
demonstrate temporal variability between pCO_2 products (Fig. 5). For most of the year, the data (Fig. 5a) stays within a
relatively narrow range (375-425 µatm), except for the summer monsoon where values can exceed 500 µatm and the median
value has its peak. In the model (Fig. 5b), pCO_2 is almost entirely above 400 µatm, with the median value increasing during
270 spring inter-monsoon and peaking in June. Similar to the data, the upper bound variability in pCO_2 peaks in August. L15 (Fig.
5c), by contrast, has a tighter envelope of variability, with 5-95 percentile values never going beyond the range of 368-434
µatm. Median pCO_2 in L15 peaks in the summer like the data, but there is no large increase in upper bound variability.

In summary, the survey of available data and comparing it to the model output produces a few distinct features: 1) available *in situ* data shows that the majority of observations are skewed towards the summer monsoon during the years 1995 and 1997; 2) most *in situ* data show CO_2 out-gassing in the AS; 3) the model has a net positive bias in surface pCO_2, driven by a joint DIC-TA bias which is slightly stronger in TA; and 4) the model captures the high summer monsoon pCO_2 values better than competing products.

3.2 pCO_2 distribution, seasonal cycle, and underlying contributors

3.2.1 Spatial pCO_2 distribution

Spatial pCO_2 anomalies from the regional mean highlight the geographic hotspots of pCO_2 inside the domain (Fig 6a). Within the regions of analysis prescribed in this study, it is clear that Oman, the Indian coast, and the North AS including the Gulf of Oman host enhanced pCO_2. In contrast, both the oligotrophic central AS and Somalia regions have negative pCO_2 anomalies. The contributing factors to these pCO_2 anomalies, temperature, DIC, TA, and freshwater components, display differing distributions. Temperature (Fig. 6c) contributes toward negative pCO_2 anomalies in a southwest-to-northeast band along the coasts of east Africa and the Arabian peninsula, up to the coasts of Pakistan and northern coast of India near Gujarat. The cold SST structure largely overlaps the stronger summer monsoon winds. The opposite trend is found in the central oligotrophic and Indian regions, where temperature contributes positively to pCO_2 anomaly, despite upwelling in the southern Indian coast. The distribution of DIC-induced anomalies (Fig. 6d) shows a positive influence near coastal regions and the western AS off the coast of Somalia, whereas a strong minimum is found in an oval region encompassing the central, open-ocean AS. TA effects (Fig. 6e) show a north-south gradient with positive contributions to pCO_2 occurring in the north and negative towards the south, in a similar distribution to surface salinity gradients in the AS. Freshwater contributions (Fig. 6f) show a similar distribution as TA, but weaker in magnitude for all regions.

Putting together all the spatial anomalies for each region, different variables become dominant (Fig. 6b). Near Oman, temperature is a strong negative factor, but it is counteracted mostly by DIC and the other effects to produce a positive anomaly. A similar pattern occurs for the North, but in this case TA and freshwater effects play a larger role than DIC. In the oligotrophic region, the strong negative DIC effect swamps all other effects. In the Somalia upwelling region, the strong positive DIC influence is stronger than opposing temperature, but TA and freshwater effects are enough to produce a slightly negative pCO_2 anomaly. The coast of India, influenced most likely by its shelf, has a very high positive DIC contribution, more than enough to overrule other variables.

3.2.2 Seasonal pCO_2 cycle

The previous section outlines why certain geographic regions within the AS have overall high or low pCO_2 values, but in order to investigate the strong seasonal monsoon impact in the AS, the decomposition of factors affecting monthly pCO_2 values is calculated at each model grid point and averaged into each analysis region (Fig. 7). Regarding the whole domain (Fig. 7a), pCO_2 variability is similar to that seen in Fig. 5b, with a spring pCO_2 peak and minimum during fall and winter. Temperature

305   effects largely mirror the overall pCO_2 cycle. DIC acts in opposition to temperature but with lower magnitude. Both TA and freshwater effects are negative for the first half of the year before becoming slightly positive in the second half. The oligotrophic central region (Fig. 7d), the largest in area, has similar pCO_2 and temperature impacts as the whole domain, with the two largely overlapping. DIC, TA, and freshwater impacts also follow similar patterns, but have slightly higher magnitudes in the central AS.

310   Different pCO_2 anomaly cycles can be found in the upwelling regions of Oman, Somalia and India (Fig. 7b,e,f). Here, a positive temperature peak appears in the spring, which is then supplanted by a positive DIC peak during the summer monsoon. In both Oman and India, the summertime DIC peak is strong enough to contribute to the annual pCO_2 peak despite cooler temperatures. In Somalia, the summertime DIC peak is not sufficiently stronger than temperature, and the maximum pCO_2 is found in the spring like in the whole domain and oligotrophic regions. Both TA and freshwater effects in these three regions

315   are lower in magnitude and generally run counter to DIC.

A completely different regime occurs in the North AS (Fig. 7c). Here, while temperature effects create a similar spring-summertime peak in pCO_2 somewhat counter-acted by DIC, during the winter monsoon temperature and DIC effects are both maximal and in opposing amplitudes. This occurs due to the convective mixing that occurs during winter in the North AS, where cooling temperatures lower pCO_2 but subsurface water introduces more DIC, resulting in a near-balance.

320   The spatial and seasonal decomposition of pCO_2 anomalies in the AS demonstrate how the four variables of DIC, TA, T, and freshwater differently impact sub-regions in the AS, on the whole and within seasons. The upwelling and coastal regions show elevated pCO_2 relative to the whole AS, which is due to enhanced DIC and counter-acted by lower temperatures. The central, oligotrophic AS has lower relative pCO_2 due to a strong negative DIC anomaly. Analyzing the seasonal cycle within the domain and its sub-regions, temperature anomalies are most responsible for pCO_2 variability, generally peaking in the

325   spring. Positive DIC contributions to seasonal pCO_2 anomalies become important in the upwelling zones during the summer monsoon, as well as the North AS due to wintertime convective mixing.

3.3   Near-surface DIC budgets and cycling

Whereas SST and its effect on pCO_2 is controlled by the physical processes of surface forcing, mixing and advection, DIC reflects both physical and biological processes because it is also impacted by photosynthesis, respiration, remineralization,

330   and shell calcification. Budgets of DIC fluxes in the upper 20 m (Fig. 8) show that two major processes dominate, vertical circulation (light blue lines) and net biological processes (green lines). In the entire domain and all sub-regions, vertical circulation (advection and mixing) acts as a source of DIC, with the sum of all biological processes acting as a sink (n.b. the top 20 m does not constitute the entire euphotic zone, so respiration and remineralization at depth is not included). Maximum magnitudes of both vertical circulation and biological flux occur during the summer monsoon for all regions, except for the

335   North AS where they occur during the winter monsoon bloom (Fig. 8c). Biological fluxes are nearly phase-matched with vertical circulation, though peaks in summer biological flux lag vertical circulation by a month (Fig. 8d,e,f). Comparing the two flux terms, after normalizing biological flux by vertical circulation flux, the relative strength of biological processes versus

vertical sources of DIC becomes apparent. In the whole domain, biological flux ranges from -90% to -34.5% of vertical flux. As a result, biological fixation of carbon is generally weaker than physical vertical delivery of DIC.

340   Air-sea flux (red lines) is always negative due to the high pCO$_2$ values, peaking during the summer monsoon. DIC flux due to atmospheric escape is mostly smaller than biological flux, with the exception of spring when primary productivity is weak and pCO$_2$ values are high. Evaporation and precipitation (brown lines) results in higher DIC for most of the year (i.e. net evaporation) in the entire domain and upwelling regions, except India where it is negative (net precipitation). The oligotrophic region's evaporation and precipitation flux (Fig. 8d) oscillates from being either positive or negative four times during the

345 year, with magnitudes rivaling air-sea flux at times. Horizontal advection (dark blue lines) is negative on average for the whole domain, denoting net export (Fig. 8a). The same pattern occurs for all sub-regions except India with net horizontal import of surface DIC (Fig. 8f). The Oman upwelling region and the oligotrophic region experience positive peaks of horizontal import during the summer monsoon, though for Somalia this period is the maximum DIC export. The overall, total flux of DIC experiences a summer positive peak during the summer monsoon, except for the North AS which has its positive peak in

350 winter.

    Overall, the near-surface AS DIC budget provides a picture where the physical delivery and biological drawdown of DIC, which are both larger in magnitude than the air-sea CO$_2$ flux, compete to produce the annual cycle of DIC fluctuations. For all regions except for the North AS (where similar processes occur during the winter monsoon), the largest physical vertical fluxes occur during the summer monsoon when wind forcing both upwells subsurface water and produces mixing to enhance

355 DIC. The biological drawdown of DIC occurs concurrently or slightly lags the physical circulation since subsurface nutrient delivery must occur before stimulating phytoplankton growth. Importantly, the magnitude of biological DIC drawdown is less than the sourcing from vertical circulation, limiting the prospect of biological control of pCO$_2$ in the AS.

3.4   Air-sea CO$_2$ flux and drivers of seasonal variability

Modeled annual mean atmospheric flux of CO$_2$ (Fig. 9a) shows outgassing (positive, red) throughout the entire domain, pro-

360 ducing an average annual CO$_2$ flux density rate of $1.9 \, \mathrm{mol \, C \, m^{-2} yr^{-1}}$ and a total of $162.6 \mathrm{TgC \, yr^{-1}}$. Similar to pCO$_2$, several hotspots appear in the geographic distribution. Near the coast of Oman, the average flux density is 2.7, with 3.2 in Somalia and 2.4 along the coast of India $\mathrm{mol \, C \, m^{-2} yr^{-1}}$, producing a flux of 11.4, 32.9, and 4.9 $\mathrm{TgCyr^{-1}}$, respectively. The other regions, the North AS and oligotrophic central AS, have average densities of 2.0 and $1.5 \, \mathrm{mol \, C \, m^{-2} yr^{-1}}$, with total fluxes of 10.5 and 28.6 $\mathrm{TgCyr^{-1}}$. The seasonal air-sea flux (Fig 9b-e) has minima during fall and winter, with an increase in spring and

365 a strong maximum during summer monsoon. Oman and Somalia flux densities during summer monsoon are 5.8 and 5.9 mol C $\mathrm{m^{-2} yr^{-1}}$, respectively. The distribution of enhanced summer air-sea CO$_2$ flux coincides with the southwest monsoon winds, as well as the band of cooler temperatures impacting spatial pCO$_2$ anomalies in Fig. 7c. The entire domain fluxes 32.0, 26.6, 90.9, and 13.1 $\mathrm{TgCyr^{-1}}$ for the winter, spring, summer, and fall periods, respectively, each contributing 19.7, 16.3, 55.9, and 8.1% of the annual total.

370   The variability in air-sea CO$_2$ flux can be attributed to the contributions of winds, pCO$_2$, and interacting cross-terms, as described in Eqn. (8). The temporal anomalies for the summer monsoon, the period with strongest CO$_2$ flux signal, are presented

in Fig. 10. Most of the domain has positive anomalies in air-sea flux (Fig. 10a). The wind contribution to flux variability, $\kappa\alpha$ (Fig. 10b), is also positive in most of the domain except the Gulf of Aden and the south-eastern corner of the domain, with its magnitude and distribution close to the total anomaly in Fig. 10a. The ΔpCO_2 contribution to seasonal flux anomaly (Fig. 10c)

375 has a lower magnitude effect overall, with positive values north of 10^oN and slightly negative to the south. Maxima in these values occur near the upwelling centers of Oman, Somalia, and the Indian coast. Second-order cross-term values (Fig. 10d) are almost all positive, with maxima also occurring near upwelling centers similar to the ΔpCO_2 term but weaker in magnitude.

The seasonal flux anomalies for all regions throughout the year are displayed in Fig. 11. The summer monsoon flux is so strong that it makes the anomalies (purple bars) for all the other seasons in all regions negative, except for the spring in the

380 North AS and central oligotrophic AS. During the winter months DJFM, both wind and pCO_2 terms produce negative flux anomalies, indicating the relative lack of winds and minimum pCO_2 values in the domain. In winter, while the negative wind term is universally strongest, within the upwelling regions the pCO_2 term is 58% of the wind term's magnitude, and 53% for the entire domain. The spring intermonsoon, where many regions such as Somalia and the central oligotrophic AS experience their pCO_2 maximum, shows a positive pCO_2 effect on flux anomaly that is as large as or larger than the negative wind effect. In the

385 oligotrophic region, the second-order cross-term is small enough so that the net result is a positive anomaly, while in Somalia the near-balance between winds and pCO_2 make the cross-terms important in creating a negative anomaly. Summer monsoon winds represent the majority contribution to CO_2 flux variability, with a minimum 64.7% contribution relative to the total anomaly in India, a maximum of 112.8% in the oligotrophic AS, and 90.8% for the whole domain. By contrast, summer pCO_2 and cross-terms contribute 6.0 and 3.1% to the domain's anomaly, respectively. Fall inter-monsoon months resemble the winter

390 monsoon, with negative wind anomalies contributing most with small or negative pCO_2 contributions. In most scenarios, pCO_2 contributes in the same direction as the winds or little at all, with the notable exceptions of Oman, oligotrophic AS, Somalia, and the domain during spring inter-monsoon.

In summary, the air-sea CO_2 flux is positive throughout the domain for the entire year, producing a total $162.6\,\mathrm{TgCyr^{-1}}$, and is particularly elevated near the upwelling regions during the summer monsoon. Seasonal variability in flux is driven primarily

395 by the strong onset of summer monsoon winds.

4 Discussion

4.1 Model pCO$_2$ vs. data

The pCO_2 output from the model has a positive bias with respect to the *in situ* data, as is clear from Fig. 3-5. The question becomes whether the model bias precludes its use in acquiring a reasonable air-sea CO_2 flux estimate. Regarding the direction

400 of CO_2 flux (positive outgassing or negative uptake), the data in Fig. 2 are clear that, to the extent that *in situ* data exist and provide good coverage, ΔpCO_2 values are mostly positive (90%). Additionally, the bias is negative in the summer months, when the overall highest pCO_2 data values occur, and also when CO_2 flux peaks due to monsoon winds. Therefore, the positive bias in model pCO_2 should not significantly change the overall direction of flux, and the model results reaffirm the previous findings of Sarma et al. (1998) and subsequent work demonstrating that the AS is a source of CO_2 to the atmosphere.

405   A positive bias in model pCO_2 has been noted in previous modeling studies. For instance, in the global data assimilation study of Valsala and Maksyutov (2010), they found an overall positive bias in the North Indian ocean, with a similar underestimate near the upwelling regions (summer negative bias in the model) of the AS and overestimate elsewhere (their Figures 3 and 4). In Sreeush et al. (2019a), ROMS resulted in systematic positive pCO_2 bias, whereas the offline Ocean Transport Tracer Model (OTTM) produced negative bias in pCO_2 in comparison to TK09. Anomalous patterns can be seen in OTTM, as well,

410   with a maximum pCO_2 found near the equator as opposed to near the Oman coast (Valsala and Murtugudde, 2015).

The search for the model bias source is hindered by the lack of *in situ* data in the region. While the bias does not appear to be from T and S, but rather DIC and TA (Fig. S4), it is difficult to pinpoint which processes create these discrepancies since in the AS domain the GLODAP database has a total of 334 locations where both DIC and TA are sampled in the upper 50m of the water column. The few available *in situ* data that *do* exist in the AS have a number of deficiencies for the purpose of validating

415   model output. First, the data available are both old and concentrated around the years 1995 and 1997. While the JGOFS studies were quintessential in diagnosing the seasonal cycle of pCO_2, they preclude being able to decipher the secular trend in surface pCO_2 due to increasing atmospheric CO_2 concentrations. In our analysis, we estimated a $+2\mu atm\ yr^{-1}$ trend, close to that of Tjiputra et al. (2014), though finding an inter-annual linear trend requires more data at regular intervals. Second, due to the nature of strong upwelling in the AS, previous cruise sampling also biases not only the summer months ($\approx$70% of data), but

420   also in the vicinity of the Oman coast (Fig. 3c). As a result, it is difficult to determine to what extent the data are representative of the entire AS. Consider that in the model, flux intensities are lower in the central, oligotrophic region (Fig. 10), but due to its surface area the total flux (28.6 $TgCyr^{-1}$) was close to that of Somalia (32.9 $TgCyr^{-1}$), an observation also made by Lendt et al. (2003). Determining to what extent the model over- or under-estimates CO_2 flux due to pCO_2 bias would require more *in situ* sampling, which would need to be designed around solving the problems of areal coverage (outside of Oman and

425   upwelling zones) and temporal coverage (off-summer months and recurrent over multiple years).

Despite the model's limitations, its advantages are also clear. Beyond the obvious increase in spatio-temporal coverage, capturing the monsoon's strong seasonal dynamics helps the model where other approaches fall short. This is especially illustrated in Fig. 5. Since upwelling regions are limited in geographic extent near the coast, capturing their high pCO_2 values can be difficult for other approaches, such as TK09 with its coarse grid. Even the L15 product, with its finer grid, is unable to

430   produce the higher pCO_2 values seen during the summer. Judging from these comparisons, the trade-off appears to be that the model currently may produce less accurate pCO_2 values outside of summer, but the explicit resolving of upwelling allows for enhanced pCO_2 values during the summer monsoon, the peak of CO_2 flux.

4.2   Surface distribution of pCO_2 and spatial, temporal anomalies

The distribution of model pCO_2 is both similar to and different from previous studies. Apart from the aforementioned bias

435   leading to heightened absolute values (though Bates et al. (2006) has >400 μatm for large parts of the AS), the relatively enhanced pCO_2 values near Oman, along the west coast of India, and in the Gulf of Aden have already been observed (Sabine et al., 2000; Bates et al., 2006; Sarma et al., 2000). These same studies, however, note a minimum of pCO_2 outside of the summer monsoon near the south-west coast of India due to freshwater influx, which is not replicated well in the model.

Additionally, elevated pCO_2 near the equator is not observed (Sabine et al., 2000; Bates et al., 2006), although as already

440 noted it can appear in other models (Valsala and Murtugudde, 2015). The model's seasonal pCO_2 minimum during the winter monsoon is also not reflective of results found elsewhere (Goyet et al. (1998a, b); Bates et al. (2006); though many studies highlight the North AS, where minimum model pCO_2 occurs during the spring). Instead, these papers state pCO_2 is minimal during the fall inter-monsoon. Likewise, the large-scale spring maximum of pCO_2 seen in the model is not found in these studies, except for in Louanchi et al. (1996), though this result is somewhat anomalous since that study showed a pCO_2

445 minimum during summer monsoon. Thus, while the model agrees with previous work insofar as the coastal regions impacted by upwelling show enhanced pCO_2, mismatches do appear in the seasonal timing of maxima and minima, especially within certain sub-regions.

The spatial decomposition of factors influencing pCO_2 (Fig. 6) highlights how geographically DIC can be the strongest factor, with temperature and TA taking secondary roles and freshwater being a weak contributor. Since DIC and TA can co-

450 vary with salinity, when they are not normalized their distribution in the AS mirrors the north-south salinity gradient (see figures 2,3 in Bates et al. (2006)). Once corrected for salinity, it is clear that the upwelling region of Oman still has elevated DIC whereas the central, oligotrophic AS shows a DIC deficit. By contrast, the onshore-offshore gradient in TA is weaker. Differences between coastal and offshore normalized DIC and TA in the AS have been previously observed (Millero et al., 1998b; Lendt et al., 2003), but the stronger relative absence of DIC in the central AS and its role in determining pCO_2

455 has not been emphasized. A similar analysis in the California Current upwelling system (Turi et al., 2014) indicates near-compensation of DIC and temperature in opposing directions, nearly overlapping each other. In that scenario, DIC overpowers temperature at the coast, with TA and freshwater being secondary. For the AS, while the upwelling regions of Oman and Somalia show temperature and DIC working against each other, they are not as well compensated. Furthermore, the gradients of positive/negative pCO_2 contributions from temperature and DIC do not overlap, leading to the curious scenario where

460 temperature and DIC both contribute positively to the pCO_2 anomaly along the Indian coast. The positioning of these gradients and the surprising negative influence of DIC away from upwelling regions perhaps underscores how the AS is rather unique, where strong seasonal upwelling winds mingle with strong tropical heating and the influence of outflows from marginal seas.

Decomposition of seasonal pCO_2 anomalies within regions portrays a slightly different picture where temperature is the dominant force, with DIC countervailing in the upwelling regions. Not only is this seasonal cycle more akin to that seen in the

465 California Current (Turi et al., 2014), the dueling role of these two forces is also reflected in a similar analysis by Sreeush et al. (2019a) for pH instead of pCO_2 in the AS. Interestingly, in that study both ROMS and OTTM were compared side-by-side, and in OTTM, TA played a larger role than in ROMS. Similarly, in Valsala and Maksyutov (2013), TA played an important role in regulating inter-annual pCO_2 variability in the AS. These results using another model raise the possibility that TA's importance is under-estimated in the current study.

470 Zooming out from the upwelling regions and looking at the whole AS, the dominance of temperature is clear. This observation, temperature overriding DIC in the AS to determine temporal pCO_2 changes, can also be seen in the interannual variability analysis of Doney et al. (2009). In the domain average, temperature effects nearly overlap with the overall pCO_2 anomaly. This result brings back into focus the seasonal timing of pCO_2 minima/maxima in the model vis à vis previous work.

In the earlier studies, which either use data directly or build statistical models from those data, there is no spring intermonsoon
475 pCO$_2$ maximum driven by heating. Indeed, Sabine et al. (2000) noted that pCO$_2$ in the spring was much lower than would be
expected given the SST, but attributed this to drawdown due to biological production. The model, however, indicates that this is
precisely the season where biological production is at its lowest. The presence of these springtime maxima can be seen in other
models, visible in the results of Valsala and Maksyutov (2010) and a synthesis by Sarma et al. (2013). Since the model indicates
temperature is producing the maxima, it reduces the concern that erroneous DIC or TA values in the model are driving this
480 signal. The model SST matches well with the *in situ* data (Fig. S4), and the forcing datasets for SST and heat flux correspond
to data that predate or include the pCO$_2$ sampling period (i.e. before 2000), so a climate change bias is unlikely. What might be
more likely, then, is a sampling bias towards summertime Oman, one of the few areas in the AS with a summertime instead of
springtime pCO$_2$ max. Such a bias could possibly obscure what is happening in the rest of the AS. Regardless, the discrepancy
between models and observations during the spring period can be added as yet another reason to conduct more *in situ* sampling
485 to either confirm or disavow whether the model results are spurious.

4.3 DIC seasonal budget and driving mechanisms

The potential for biological control in setting pCO$_2$ has been found in Sri Lanka near the AS (Chakraborty et al., 2018). In this
study, it was found that the source water in Sri Lanka was sufficiently low in DIC relative to inorganic nutrients that upwelling
actually reduced surface pCO$_2$. In a similar vein, Takahashi et al. (2002) found, using a metric comparing temperature and
490 "biological" effects (i.e. everything else), that the AS's pCO$_2$ is reduced more by biological production than temperature
effects. Conducting this analysis on the model output (Fig. S5), it appears that "biological" control appears dominant over
the upwelling areas (Oman coast, coast of Somalia, India) and near the equator east of 60°E, but for the majority of the AS
temperature dominates. This cursory analysis aside, as is evident in the results of Chakraborty et al. (2018), the more useful
comparison is in determining whether biological production is sufficient to outweigh DIC enhancement from subsurface water.
495   In summary, the results in Fig. 8 indicate that for the entire AS, DIC enhancement by vertical circulation (both advection
and mixing) brings more DIC into the near-surface than is removed by net biological processes, and so no biologically-induced
decrease of pCO$_2$ occurs. The timing of biological drawdown, occurring at the same time or lagging vertical circulation,
is consistent with the general phenology of blooms and similar to previous findings (Louanchi et al., 1996; Rixen et al.,
2006; Sharada et al., 2008). The result that biological cycling of carbon is much larger than the air-sea flux of CO$_2$ also
500 corroborates the results of Lendt et al. (2003), who found net community production to be ≈3.6 times larger than CO$_2$ emission.
The relatively low impact of horizontal advection is an interesting detail to consider; in other upwelling systems, significant
proportions of water and biological production are advected offshore (Nagai et al., 2015). Lendt et al. (2003) suggest upwelled
nitrate is assimilated and does not arrive in the central AS, while Resplandy et al. (2011) show that a large fraction of total
nutrients in the central AS come from the upwelling zones. Thus, although water may be advected offshore, the relevant
505 timescale for DIC cycling processes (i.e. air-sea emission, biological uptake) may be short enough so that horizontal export of
enhanced DIC (keep in mind the onshore-offshore normalized DIC gradient) from the upwelling regions does not significantly
contribute to the central AS or other regions.

4.4 Variability and mechanisms controlling air-sea CO_2 flux

4.4.1 Flux distribution, seasonality, and drivers

510 The model results both affirm the conclusions of previous studies in terms of CO_2 flux direction and seasonality, yet find difference in magnitudes. As previously stated, the AS is a atmospheric CO_2 source, with most flux occurring (56%) during the summer monsoon (Fig. 9). In our results, however, there is no region during any of the seasons where uptake of CO_2 takes place. While somewhat expected, this is still in disagreement with some of the other pCO_2 datasets previously considered, such as in Sarma (2003), where negative ΔpCO_2 values appear, such as during winter monsoon near the south coast of India. The

515 model's positive pCO_2 bias may be to blame for this, making it so that no negative ΔpCO_2 appears. Despite the positive pCO_2 bias, a few other patterns are clear in comparison to other CO_2 flux estimates. Sabine et al. (2000) and Sarma (2003) both find the maximum flux occurring during the summer monsoon centered around the upwelling regions, which is also quite visible in the model results (Fig. 10d). However, Bates et al. (2006) found that a secondary maximum of flux occurs during the winter monsoon, though due to the color scale in their figure 6 it is difficult to ascertain much beyond CO_2 outgassing from the AS

520 during all months of the year. Their secondary max in flux may be partly attributable to higher wintertime pCO_2, as well.

The fact that model CO_2 flux peaks in summer despite a wide-ranging spring peak in pCO_2 is the first sign that perhaps pCO_2 is not the primary driver in determining flux timing. The Reynolds decomposition of CO_2 flux terms (Fig. 10) clearly shows that a large proportion of the summer flux is due to the arrival of the strong SW summer monsoon winds. The positive contributions due to pCO_2 occur in the usual upwelling regions, though their contribution in magnitude is relatively muted, and

525 negative in the southern portion of the AS. Cross-terms, while non-zero, are inconsequential in determining the overall anomaly in summer flux intensity, as has been seen elsewhere (Doney et al., 2009). Indeed, one of the largest cross-term contributions is in Oman during the summer (Fig. 11), but this clearly is not enough to sway the direction of the anomaly. The summer flux signal is so strong that in nearly all the regions outside of summer, the anomaly is negative (Fig. 11). Furthermore, the contribution of winds in particular is so strong, it is the largest factor all year except for the spring intermonsoon, where peak

530 pCO_2 is important relative to the effects of wind (or lack thereof) in the central oligotrophic AS, Somalia, and the averaged domain. This would suggest that, on first order, winds are the most important factor in determining the seasonal air-sea flux cycle in the AS, to the point that wind contribution to the domain's summer anomaly was 90.8% in magnitude relative to the total. Therefore, when considering the inconsistencies of models in estimating air-sea CO_2 flux (Sarma et al., 2013), the possibility that incomplete representation of winds and the various parameterizations of piston velocity must be considered in

535 addition to pCO_2.

4.4.2 Influence of variable pCO_2 in flux magnitude

While strong monsoon winds dominate the timing of air-sea CO_2 flux, and the AS is always a source of CO_2 due to mostly positive ΔpCO_2, the variability in pCO_2 between independent sources can still result in a wide range of overall magnitudes. In the AS, CO_2 outgassing estimates vary from 7 TgCyr^{-1} (Goyet et al., 1998b) to >90 TgCyr^{-1} (Sarma, 2003), with each study

540 using their own pCO_2 data and wind parameterizations. Considering the important role of winds, the best way to investigate the

role of pCO_2 variability is to keep winds (and their flux parameterization) constant. Towards this end, we use multiple pCO_2 products to calculate CO_2 flux with the same winds and parameterization as the model (Fig. 12). As summarized in Table 1, pCO_2 from TK09, L15, GLODAP data and Sarma (2003), interpolated to the WOA 1^ox1^o grid, were used in these calculations (except for TK09 where the coarse resolution reduced coverage). The original applicability of the Sarma (2003) model is north

545   of 10^oN, and so flux was calculated for this region, as well.

Despite differing pCO_2 seasonality (Fig. 5), all calculations have their peak CO_2 flux sometime in the summer, confirming the role of winds in CO_2 flux timing. After calculating total flux for both the entire AS and the Sarma (2003) reduced domain, this study's model consistently produced one of the higher estimates (except for GLODAP in the reduced domain; Fig. 12b). This is perhaps unsurprising, considering the pCO_2 bias. The ratio between the largest and smallest estimates of total CO_2 flux

550   is 2.1 (57-120 $TgCyr^{-1}$) for the whole domain, and 5.3 (12.3 and 65.6 $TgCyr^{-1}$) for the reduced domain. It should be noted that application of the Sarma (2003) model resulted in negative ΔpCO_2 values. While some negative values were reported in the original publication, the total fluxes (12.3 or 17.6 $TgCyr^{-1}$) were quite smaller than the 70 $TgCyr^{-1}$ reported using the same parameterization from Wanninkhof (1992). Removing the two Sarma models from the reduced domain analysis produces a ratio of 1.6 between the largest and smallest flux values, more in line with the whole domain's variability. Additionally, the

555   GLODAP data, with no temporal variability in pCO_2, probably over-estimate pCO_2 and hence flux due to sampling bias near Oman during the summer monsoon, and so the ratio between flux estimates may indeed be smaller. As a final note, another interesting detail concerns how the original estimate of Sarma (2003) at 70 $TgCyr^{-1}$ is larger than both the model, which had 57.1 $TgCyr^{-1}$, and GLODAP data. Thus, while the model pCO_2 bias makes us think the model over-estimates flux, it is still within the range of previous studies in the AS.

560   Ultimately, once winds are controlled, it appears that on balance: 1) gridded data-based pCO_2 products will under-estimate the upwelling zone maxima of pCO_2 and CO_2 flux during the summer, 2) the model over-estimates pCO_2 the rest of the year, eventually contributing to a possible over-estimate of CO_2 flux, and 3) this leaves reality somewhere in between. The only way to rectify these differences and arrive at a more accurate estimate will be to conduct sufficient *in situ* sampling of DIC, TA, and pCO_2 in more regions than the upwelling zones, and preferably outside of the summer and over the course of multiple

565   years. With the advent of ARGO floats with pH sensors, and the advancement of technology for other variables such as TA, the possibility emerges of using autonomous sampling platforms to expand beyond the limitations of ship-board measurements to fill the data gap in the AS carbon system.

5 Conclusions

In this study, we used a regional circulation model coupled with a biogeochemical model to investigate the annual magnitude,

570   seasonal cycle, and drivers of air-sea CO_2 flux in the AS, primarily winds and pCO_2. This effort was made to complement previous flux estimates, where limited data or insufficient model resolution have produced contrasting results. Consistent with previous work, we find that the AS is a source of CO_2 to the atmosphere for the entire year, with the bulk occurring during the summer monsoon. Our estimate of flux, $\approx$160 $TgCyr^{-1}$, with concentrated flux densities up to 6 $molCm^{-2}yr^{-1}$ in the

upwelling regions, is larger than most previous reports but not inconsistent with the range of other findings. Since the AS lacks

575   carbon data, here we subjected the model to validation with raw data instead of smoothed climatologies. The model is shown to have a positive bias in pCO_2, attributed to TA and DIC, with TA bias being stronger. Despite this, pCO_2 variability compares favorably to alternative products in the region. The bias results in strongly positive ΔpCO_2 throughout the domain year-round. While positive ΔpCO_2 values have been observed before in the AS, we likely over-estimate CO_2 flux outside of the summer monsoon.

580   The majority of flux occurs during the summer as opposed to a modeled spring pCO_2 maximum due to the influence of winds. A Reynolds decomposition of both pCO_2 and wind variability shows that the intense winds of the summer monsoon contribute 90% of that season's flux anomaly. In fact, winds play a more important role than the increase of pCO_2 in the upwelling regions. Even though winds represent such a major variable in determining AS CO_2 flux *timing*, the variability in *total* flux due to different pCO_2 products leads to a 2x range in magnitude. These results suggest that in addition to the expected

585   increase of surface ocean pCO_2 due to anthropogenic climate change, possible changes in the timing, location, and magnitude of monsoon winds (Lachkar et al., 2018; Praveen et al., 01 Apr. 2020) will have downstream impacts on seasonal air-sea flux.

An important result of this modeling study is that temperature drives a springtime maximum of pCO_2 in the AS. This maximum has been observed in lower-resolution models, but is not found in the *in situ* data. Due to the fact that temperature is not sensitive to biological processes like DIC and TA, this discrepancy suggests that more sampling is necessary to deter-

590   mine whether it is an artifact of spotty sampling or an inherent problem in models unrelated to resolving coastal upwelling. Additionally, we find that spatial gradients of DIC and temperature do not overlap as they do elsewhere in the ocean. Instead, temperature follows a southwest-northeast monsoon wind pattern, whereas DIC is enhanced nearest to the coasts. The resulting apparent deficit of normalized DIC in the central, oligotrophic AS has not been emphasized previously. Finally, we find that despite the intense biological activity in the AS, primary production by phytoplankton is insufficient to counter the increased

595   carbon supply provided by vertical circulation during bloom periods.

Models can be used to expand spatiotemporal coverage when data is scarce. However, models' limitations often manifest when there is no new data to test their fidelity. Limitations in the spatiotemporal coverage of existing datasets stem from biases in sampling during summer monsoon, sampling close to the Oman upwelling region, and limited in scope to the years of JGOFS expeditions of the 1990s. In order to fully characterize the pCO_2 cycle outside of summer in the rest of the AS, as well

600   as to determine the secular trend of surface pCO_2 due to anthropogenic carbon additions to the atmosphere, more *in situ* data of the carbon system (e.g. DIC, TA, pCO_2), from shipboard measurements or autonomous sampling platforms, are sorely needed. Furthermore, since ΔpCO_2 is generally positive in the AS, the direction of air-sea CO_2 exchange examined here is robust to model error, whereas other important indicators such as pH and its relevant biological thresholds will be less so. These data are thus critical for resolving the possible responses of the carbon system in the AS to ongoing climate change, whether from

605   changes in timing or magnitude of monsoon wind forcing, the impact of increased surface heating on stratification and vertical circulation, or changing levels of primary and fisheries productivity with altered carbonate solubility. Without this baseline information, it will be difficult to predict what the future has in store for the AS carbon system.

Competing interests. The authors declare that they have no competing financial interests.

Acknowledgements. Support for this research comes from the Center for Prototype Climate Modeling (CPCM), the New York University
610 Abu Dhabi (NYUAD) Research Institute. Computations were conducted at the High Performance cluster (HPC) at NYUAD, Dalma. We
deeply thank both B. Marchand and M. Barwani for their technical support.

References

Bakker, D. C., Pfeil, B., Landa, C. S., Metzl, N., O'brien, K. M., Olsen, A., Smith, K., Cosca, C., Harasawa, S., Jones, S. D., et al.: A multi-decade record of high-quality fCO (2) data in version 3 of the Surface Ocean CO2 Atlas (SOCAT), Earth System Science Data, 8, 383–413, 2016.

Bates, N. R., Pequignet, A. C., and Sabine, C. L.: Ocean carbon cycling in the Indian Ocean: 1. Spatiotemporal variability of inorganic carbon and air-sea CO2 gas exchange, Global Biogeochemical Cycles, 20, https://doi.org/10.1029/2005GB002491, https://agupubs.onlinelibrary.wiley.com/doi/abs/10.1029/2005GB002491, 2006.

Carton, J. A. and Giese, B. S.: A reanalysis of ocean climate using Simple Ocean Data Assimilation (SODA), Monthly weather review, 136, 2999–3017, 2008.

Casey, K. S. and Cornillon, P.: A comparison of satellite and in situ–based sea surface temperature climatologies, Journal of Climate, 12, 1848–1863, 1999.

Chakraborty, K., Valsala, V., Gupta, G., and Sarma, V.: Dominant biological control over upwelling on pCO2 in sea east of Sri Lanka, Journal of Geophysical Research: Biogeosciences, 123, 3250–3261, 2018.

Ciais, P., Sabine, C., Bala, G., Bopp, L., Brovkin, V., Canadell, J., Chhabra, A., DeFries, R., Galloway, J., Heimann, M., et al.: Climate change 2013: the physical science basis. Contribution of Working Group I to the Fifth Assessment Report of the Intergovernmental Panel on Climate Change, K., Tignor, M., Allen, SK, Boschung, J., Nauels, A., Xia, Y., Bex, V., Midgley, PM, Eds, 2013.

da Silva, A. M., Young, C. C., and Levitus, S.: Atlas of surface marine data 1994, Vol. 4: Anomalies of fresh water fluxes, NOAA Atlas, NESDIS, 9, 1994.

Dickson, A. and Millero, F. J.: A comparison of the equilibrium constants for the dissociation of carbonic acid in seawater media, Deep Sea Research Part A. Oceanographic Research Papers, 34, 1733–1743, 1987.

Doney, S. C., Lima, I., Feely, R. A., Glover, D. M., Lindsay, K., Mahowald, N., Moore, J. K., and Wanninkhof, R.: Mechanisms governing interannual variability in upper-ocean inorganic carbon system and air–sea CO2 fluxes: Physical climate and atmospheric dust, Deep Sea Research Part II: Topical Studies in Oceanography, 56, 640–655, 2009.

Goyet, C., Metzl, N., Millero, F., Eischeid, G., O'sullivan, D., and Poisson, A.: Temporal variation of the sea surface CO2/carbonate properties in the Arabian Sea, Marine Chemistry, 63, 69–79, 1998a.

Goyet, C., Millero, F. J., O'Sullivan, D., Eischeid, G., McCue, S., and Bellerby, R.: Temporal variations of pCO2 in surface seawater of the Arabian Sea in 1995, Deep Sea Research Part I: Oceanographic Research Papers, 45, 609–623, 1998b.

Gruber, N., Frenzel, H., Doney, S. C., Marchesiello, P., McWilliams, J. C., Moisan, J. R., Oram, J. J., Plattner, G.-K., and Stolzenbach, K. D.: Eddy-resolving simulation of plankton ecosystem dynamics in the California Current System, Deep Sea Research Part I: Oceanographic Research Papers, 53, 1483–1516, 2006.

Gruber, N., Lachkar, Z., Frenzel, H., Marchesiello, P., Münnich, M., McWilliams, J. C., Nagai, T., and Plattner, G.-K.: Eddy-induced reduction of biological production in eastern boundary upwelling systems, Nature geoscience, 4, 787–792, 2011.

Gruber, N., Hauri, C., Lachkar, Z., Loher, D., Frölicher, T. L., and Plattner, G.-K.: Rapid progression of ocean acidification in the California Current System, science, 337, 220–223, 2012.

Hauri, C., Gruber, N., Vogt, M., Doney, S. C., Feely, R. A., Lachkar, Z., Leinweber, A., McDonnell, A. M., Münnich, M., and Plattner, G.-K.: Spatiotemporal variability and long-term trends of ocean acidification in the California Current System, Biogeosciences, 10, 193–216, 2013.

Hood, R. R., Urban, E. R., McPhaden, M. J., Su, D., and Raes, E.: The 2nd International Indian Ocean Expedition (IIOE-2): Motivating New
650   Exploration in a Poorly Understood Basin., Limnology and Oceanography Bulletin, 25, 117–124, 2016.

Keeling, C. D.: Carbon dioxide in surface ocean waters: 4. Global distribution, Journal of Geophysical Research (1896-1977), 73, 4543–4553,
    https://doi.org/10.1029/JB073i014p04543, https://agupubs.onlinelibrary.wiley.com/doi/abs/10.1029/JB073i014p04543, 1968.

Keeling, C. D., Brix, H., and Gruber, N.: Seasonal and long-term dynamics of the upper ocean carbon cycle at Station ALOHA near Hawaii,
    Global Biogeochemical Cycles, 18, 2004.

655   Khatiwala, S., Primeau, F., and Hall, T.: Reconstruction of the history of anthropogenic CO$_2$ concentrations in the ocean, Nature, 462,
    346–349, 2009.

Kumar, S. P., Ramaiah, N., Gauns, M., Sarma, V., Muraleedharan, P., Raghukumar, S., Kumar, M. D., and Madhupratap, M.: Physical
    forcing of biological productivity in the Northern Arabian Sea during the Northeast Monsoon, Deep Sea Research Part II: Topical Studies
    in Oceanography, 48, 1115–1126, 2001.

660   Lachkar, Z. and Gruber, N.: Response of biological production and air–sea CO2 fluxes to upwelling intensification in the California and
    Canary Current Systems, Journal of Marine Systems, 109, 149–160, 2013.

Lachkar, Z., Smith, S., Lévy, M., and Pauluis, O.: Eddies reduce denitrification and compress habitats in the Arabian Sea, Geophysical
    Research Letters, 43, 9148–9156, 2016.

Lachkar, Z., Lévy, M., and Smith, S.: Intensification and deepening of the Arabian Sea oxygen minimum zone in response to increase in
665   Indian monsoon wind intensity., Biogeosciences, 15, 2018.

Landschützer, P., Gruber, N., Haumann, F. A., Rödenbeck, C., Bakker, D. C., Van Heuven, S., Hoppema, M., Metzl, N., Sweeney, C.,
    Takahashi, T., et al.: The reinvigoration of the Southern Ocean carbon sink, Science, 349, 1221–1224, 2015.

Large, W. G., McWilliams, J. C., and Doney, S. C.: Oceanic vertical mixing: A review and a model with a nonlocal boundary layer parame-
    terization, Reviews of Geophysics, 32, 363–403, 1994.

670   Lee, K., Tong, L. T., Millero, F. J., Sabine, C. L., Dickson, A. G., Goyet, C., Park, G.-H., Wanninkhof, R., Feely, R. A., and Key, R. M.:
    Global relationships of total alkalinity with salinity and temperature in surface waters of the world's oceans, Geophysical Research Letters,
    33, https://doi.org/10.1029/2006GL027207, https://agupubs.onlinelibrary.wiley.com/doi/abs/10.1029/2006GL027207, 2006.

Lendt, R., Thomas, H., Hupe, A., and Ittekkot, V.: Response of the near-surface carbonate system of the northwestern Arabian Sea to the
    southwest monsoon and related biological forcing, Journal of Geophysical Research: Oceans, 108, 2003.

675   Lévy, M., Shankar, D., André, J.-M., Shenoi, S., Durand, F., and de Boyer Montégut, C.: Basin-wide seasonal evolution of the Indian Ocean's
    phytoplankton blooms, Journal of Geophysical Research: Oceans, 112, 2007.

Louanchi, F., Metzl, N., and Poisson, A.: Modelling the monthly sea surface fCO2 fields in the Indian Ocean, Marine Chemistry, 55, 265–279,
    1996.

Lovenduski, N. S., Gruber, N., Doney, S. C., and Lima, I. D.: Enhanced CO2 outgassing in the Southern Ocean from a positive phase of the
680   Southern Annular Mode, Global Biogeochemical Cycles, 21, 2007.

Mahadevan, A., Lévy, M., and Mémery, L.: Mesoscale variability of sea surface pCO2: What does it respond to?, Global Biogeochemical
    Cycles, 18, https://doi.org/10.1029/2003GB002102, https://agupubs.onlinelibrary.wiley.com/doi/abs/10.1029/2003GB002102, 2004.

Mahadevan, A., Tagliabue, A., Bopp, L., Lenton, A., Mémery, L., and Lévy, M.: Impact of episodic vertical fluxes on sea surface
    pCO$_2$, Philosophical Transactions of the Royal Society A: Mathematical, Physical and Engineering Sciences, 369, 2009–
685   2025, https://doi.org/10.1098/rsta.2010.0340, https://royalsocietypublishing.org/doi/abs/10.1098/rsta.2010.0340, 2011.

Marchesiello, P., Debreu, L., and Couvelard, X.: Spurious diapycnal mixing in terrain-following coordinate models: The problem and a solution, Ocean Modelling, 26, 156–169, 2009.

Mehrbach, C., Culberson, C., Hawley, J., and Pytkowicx, R.: Measurement of the apparent dissociation constants of carbonic acid in seawater at atmospheric pressure 1, Limnology and oceanography, 18, 897–907, 1973.

690 Millero, F. J.: Thermodynamics of the carbon dioxide system in the oceans, Geochimica et Cosmochimica Acta, 59, 661–677, 1995.

Millero, F. J., Degler, E. A., O'Sullivan, D. W., Goyet, C., and Eischeid, G.: The carbon dioxide system in the Arabian Sea, Deep Sea Research Part II: Topical Studies in Oceanography, 45, 2225–2252, 1998a.

Millero, F. J., Lee, K., and Roche, M.: Distribution of alkalinity in the surface waters of the major oceans, Marine Chemistry, 60, 111 – 130, https://doi.org/https://doi.org/10.1016/S0304-4203(97)00084-4, http://www.sciencedirect.com/science/article/pii/S0304420397000844, 1998b.

695 S0304420397000844, 1998b.

Nagai, T., Gruber, N., Frenzel, H., Lachkar, Z., McWilliams, J. C., and Plattner, G.-K.: Dominant role of eddies and filaments in the offshore transport of carbon and nutrients in the C alifornia C urrent S ystem, Journal of Geophysical Research: Oceans, 120, 5318–5341, 2015.

Naqvi, S. W. A., Gupta, R. S., and Kumar, M. D.: Carbon dioxide and nitrous oxide in the Arabian Sea, Washington DC American Geophysical Union Geophysical Monograph Series, 75, 85–92, https://doi.org/10.1029/GM075p0085, 1993.

700 Naqvi, S. W. A., Bange, H. W., Gibb, S. W., Goyet, C., Hatton, A. D., and Upstill-Goddard, R. C.: Biogeochemical ocean-atmosphere transfers in the Arabian Sea, Progress in Oceanography, 65, 116–144, 2005.

Olsen, A., Lange, N., Key, R. M., Tanhua, T., Álvarez, M., Becker, S., Bittig, H. C., Carter, B. R., Cotrim da Cunha, L., Feely, R. A., van Heuven, S., Hoppema, M., Ishii, M., Jeansson, E., Jones, S. D., Jutterström, S., Karlsen, M. K., Kozyr, A., Lauvset, S. K., Lo Monaco, C., Murata, A., Pérez, F. F., Pfeil, B., Schirnick, C., Steinfeldt, R., Suzuki, T., Telszewski, M., Tilbrook, B., Velo, A., and Wanninkhof, R.:

705 GLODAPv2.2019 – an update of GLODAPv2, Earth System Science Data, 11, 1437–1461, https://doi.org/10.5194/essd-11-1437-2019, https://essd.copernicus.org/articles/11/1437/2019/, 2019.

Orr, J. and Epitalon, J.-M.: Improved routines to model the ocean carbonate system: mocsy 2.0., Geoscientific Model Development, 8, 2015.

Orr, J. C., Epitalon, J.-M., Dickson, A. G., and Gattuso, J.-P.: Routine uncertainty propagation for the marine carbon dioxide system, Marine Chemistry, 207, 84–107, 2018.

710 Paulmier, A., Ruiz-Pino, D., and Garçon, V.: CO_2 maximum in the oxygen minimum zone (OMZ), Biogeosciences, 8, 239–252, https://doi.org/10.5194/bg-8-239-2011, https://bg.copernicus.org/articles/8/239/2011/, 2011.

Pfeil, B., Olsen, A., Bakker, D. C., Hankin, S., Koyuk, H., Kozyr, A., Malczyk, J., Manke, A., Metzl, N., Sabine, C. L., et al.: A uniform, quality controlled Surface Ocean CO 2 Atlas (SOCAT), Earth System Science Data, 5, 125–143, 2013.

Praveen, V., Valsala, V., Ajayamohan, R. S., and Balasubramanian, S.: Oceanic Mixing over the Northern Arabian Sea in a Warming Scenario:

715 Tug of War between Wind and Buoyancy Forces, Journal of Physical Oceanography, 50, 945 – 964, https://doi.org/10.1175/JPO-D-19-0173.1, https://journals.ametsoc.org/view/journals/phoc/50/4/jpo-d-19-0173.1.xml, 01 Apr. 2020.

Resplandy, L., Lévy, M., Madec, G., Pous, S., Aumont, O., and Kumar, D.: Contribution of mesoscale processes to nutrient budgets in the Arabian Sea, Journal of Geophysical Research: Oceans, 116, 2011.

Resplandy, L., Lévy, M., and McGillicuddy Jr., D. J.: Effects of Eddy-Driven Subduction on Ocean Biological Carbon Pump, Global Bio-

720 geochemical Cycles, 33, 1071–1084, https://doi.org/10.1029/2018GB006125, https://agupubs.onlinelibrary.wiley.com/doi/abs/10.1029/2018GB006125, 2019.

Risien, C. M. and Chelton, D. B.: A global climatology of surface wind and wind stress fields from eight years of QuikSCAT scatterometer data, Journal of Physical Oceanography, 38, 2379–2413, 2008.

Rixen, T., Goyet, C., and Ittekkot, V.: Diatoms and their influence on the biologically mediated uptake of atmospheric CO 2 in the Arabian
Sea upwelling system, Biogeosciences, 3, 1–13, 2006.

Sabine, C., Wanninkhof, R., Key, R., Goyet, C., and Millero, F. J.: Seasonal CO2 fluxes in the tropical and subtropical Indian Ocean, Marine
Chemistry, 72, 33–53, 2000.

Sarma, V.: Monthly variability in surface pCO2 and net air-sea CO2 flux in the Arabian Sea, Journal of Geophysical Research: Oceans, 108,
2003.

Sarma, V., Kumar, M. D., and George, M.: The central and eastern Arabian Sea as a perennial source of atmospheric carbon dioxide, Tellus
B: Chemical and Physical Meteorology, 50, 179–184, 1998.

Sarma, V., Swathi, P., Kumar, M. D., Prasannakumar, S., Bhattathiri, P., Madhupratap, M., Ramaswamy, V., Sarin, M., Gauns, M., Ramaiah,
N., et al.: Carbon budget in the eastern and central Arabian Sea: An Indian JGOFS synthesis, Global Biogeochemical Cycles, 17, 2003.

Sarma, V. V., S, S., Kumar, M. D., Gauns, M., and Madhupratap, M.: Seasonal controls on surface pCO 2 in the central and east-
ern Arabian Sea, Academy Proceedings in Earth and Planetary Sciences, 109, 471–479, http://proxy.library.nyu.edu/login?url=https:
//www.proquest.com/docview/214115753?accountid=12768, copyright - Indian Academy of Sciences 2000; Last updated - 2010-08-11;
SubjectsTermNotLitGenreText - Arabian Sea, 2000.

Sarma, V. V. S. S., Lenton, A., Law, R. M., Metzl, N., Patra, P. K., Doney, S., Lima, I. D., Dlugokencky, E., Ramonet, M., and Valsala, V.:
Sea–air CO₂ fluxes in the Indian Ocean between 1990 and 2009, Biogeosciences, 10, 7035–7052, https://doi.org/10.5194/bg-10-7035-
2013, https://bg.copernicus.org/articles/10/7035/2013/, 2013.

Schott, F. A. and McCreary Jr, J. P.: The monsoon circulation of the Indian Ocean, Progress in Oceanography, 51, 1–123, 2001.

Sharada, M., Swathi, P., Yajnik, K., and Devasena, C. K.: Role of biology in the air-sea carbon flux in the Bay of Bengal and Arabian Sea,
Journal of earth system science, 117, 429–447, 2008.

Shchepetkin, A. F. and McWilliams, J. C.: The regional oceanic modeling system (ROMS): a split-explicit, free-surface, topography-
following-coordinate oceanic model, Ocean modelling, 9, 347–404, 2005.

Smith, S. L.: The Arabian Sea of the 1990s: New biogeochemical understanding, Progress in Oceanography, 2, 113–115, 2005.

Sreeush, M. G., Rajendran, S., Valsala, V., Pentakota, S., Prasad, K., and Murtugudde, R.: Variability, trend and controlling factors of Ocean
acidification over Western Arabian Sea upwelling region, Marine Chemistry, 209, 14–24, 2019a.

Sreeush, M. G., Valsala, V., Santanu, H., Pentakota, S., Prasad, K., Naidu, C., and Murtugudde, R.: Biological production in the Indian Ocean
upwelling zones-Part 2: Data based estimates of variable compensation depth for ocean carbon models via cyclo-stationary Bayesian
Inversion., Deep Sea Research Part II: Topical Studies in Oceanography, p. 104619, 2019b.

Takahashi, T., Sutherland, S. C., Sweeney, C., Poisson, A., Metzl, N., Tilbrook, B., Bates, N., Wanninkhof, R., Feely, R. A., Sabine, C.,
et al.: Global sea–air CO2 flux based on climatological surface ocean pCO2, and seasonal biological and temperature effects, Deep Sea
Research Part II: Topical Studies in Oceanography, 49, 1601–1622, 2002.

Takahashi, T., Sutherland, S. C., Wanninkhof, R., Sweeney, C., Feely, R. A., Chipman, D. W., Hales, B., Friederich, G., Chavez, F., Sabine,
C., et al.: Climatological mean and decadal change in surface ocean pCO2, and net sea–air CO2 flux over the global oceans, Deep Sea
Research Part II: Topical Studies in Oceanography, 56, 554–577, 2009.

Takahashi, T., Sutherland, S. C., and Kozyr, A.: Global Ocean Surface Water Partial Pressure of CO2 Database: Measurements Performed
During 1957-2018 (LDEO Database Version 2018) (NCEI Accession 0160492)., https://doi.org/10.3334/cdiac/otg.ndp088(v2015), 2019.

Taylor, K. E.: Summarizing multiple aspects of model performance in a single diagram, Journal of Geophysical Research: Atmospheres, 106,
7183–7192, 2001.

Tjiputra, J. F., Olsen, A., Bopp, L., Lenton, A., Pfeil, B., Roy, T., Segschneider, J., Totterdell, I., and Heinze, C.: Long-term surface pCO2 trends from observations and models, Tellus B: Chemical and Physical Meteorology, 66, 23 083, 2014.

Turi, G., Lachkar, Z., and Gruber, N.: Spatiotemporal variability and drivers of pCO2 and air–sea CO2 fluxes in the California Current
765   System: an eddy-resolving modeling study, Biogeosciences, 11, 671–690, 2014.

Valsala, V. and Maksyutov, S.: Simulation and assimilation of global ocean pCO2 and air–sea CO2 fluxes using ship observations of surface ocean pCO2 in a simplified biogeochemical offline model, Tellus B: Chemical and Physical Meteorology, 62, 821–840, 2010.

Valsala, V. and Maksyutov, S.: Interannual variability of the air–sea CO 2 flux in the north Indian Ocean, Ocean Dynamics, 63, 165–178, 2013.

770   Valsala, V. and Murtugudde, R.: Mesoscale and intraseasonal air–sea CO2 exchanges in the western Arabian Sea during boreal summer, Deep Sea Research Part I: Oceanographic Research Papers, 103, 101–113, 2015.

Valsala, V., Sreeush, M. G., and Chakraborty, K.: The IOD Impacts on the Indian Ocean Carbon Cycle, Journal of Geophysical Research: Oceans, 125, e2020JC016 485, https://doi.org/https://doi.org/10.1029/2020JC016485, https://agupubs.onlinelibrary.wiley.com/doi/abs/10. 1029/2020JC016485, e2020JC016485 2020JC016485, 2020.

775   Van Heuven, S., Pierrot, D., Rae, J., Lewis, E., and Wallace, D.: MATLAB program developed for CO2 system calculations, ORNL/CDIAC-105b. Carbon Dioxide Information Analysis Center, Oak Ridge National Laboratory, US Department of Energy, Oak Ridge, Tennessee, 530, 2011.

Vic, C., Roullet, G., Carton, X., and Capet, X.: Mesoscale dynamics in the Arabian Sea and a focus on the Great Whirl life cycle: A numerical investigation using ROMS, Journal of Geophysical Research: Oceans, 119, 6422–6443, https://doi.org/10.1002/2014JC009857,
780   https://agupubs.onlinelibrary.wiley.com/doi/abs/10.1002/2014JC009857, 2014.

Wanninkhof, R.: Relationship between wind speed and gas exchange over the ocean, Journal of Geophysical Research: Oceans, 97, 7373–7382, 1992.

Weiss, R.: Carbon dioxide in water and seawater: the solubility of a non-ideal gas, Marine chemistry, 2, 203–215, 1974.

Wolf-Gladrow, D. A., Zeebe, R. E., Klaas, C., Körtzinger, A., and Dickson, A. G.: Total alkalinity: The explicit conservative expression and
785   its application to biogeochemical processes, Marine Chemistry, 106, 287–300, 2007.
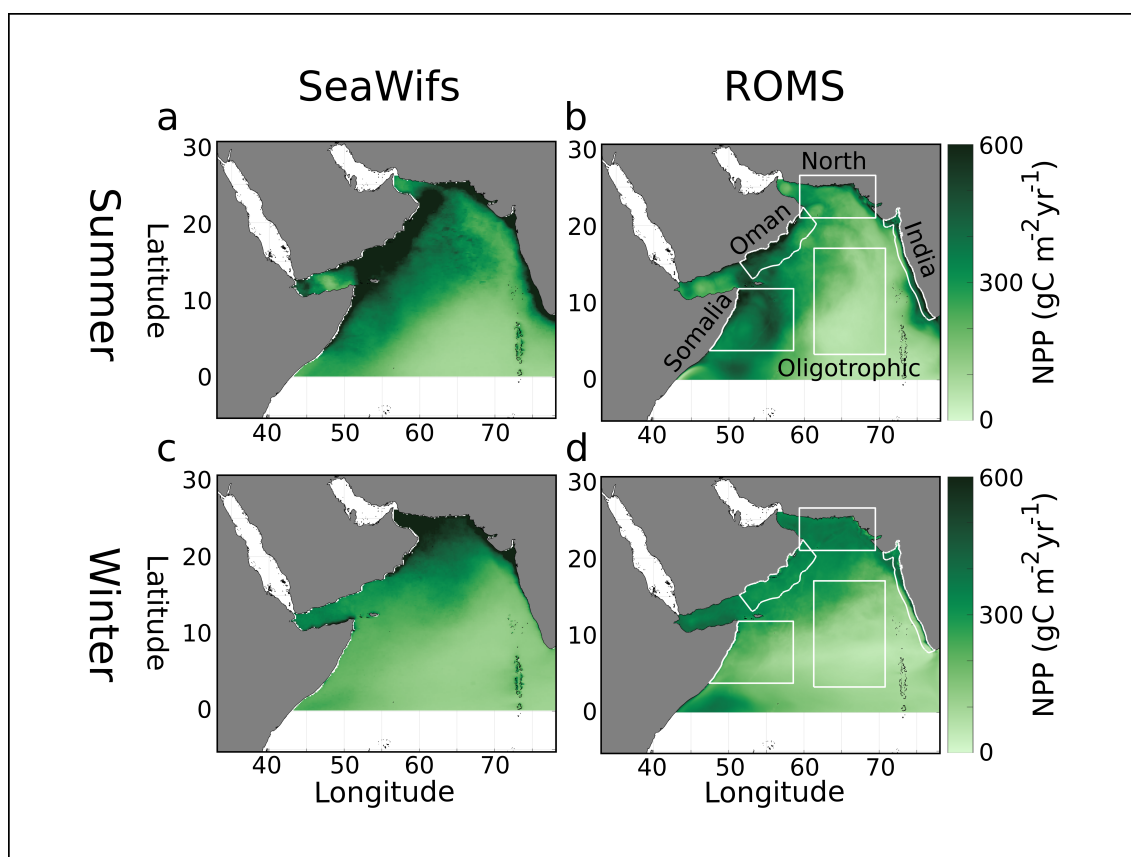
Figure 1. Vertically integrated net primary production in the Arabian Sea $gCm^{-2}yr^{-1}$ from the VGPM algorithm (Behrenfeld and Falkowski, 1997) for SeaWifs (a,c) and model output (b,d) for the summer (JJAS, a-b) and winter (DJFM,c-d) monsoon. White boxes in (b,d) denote regions of analysis in the paper.
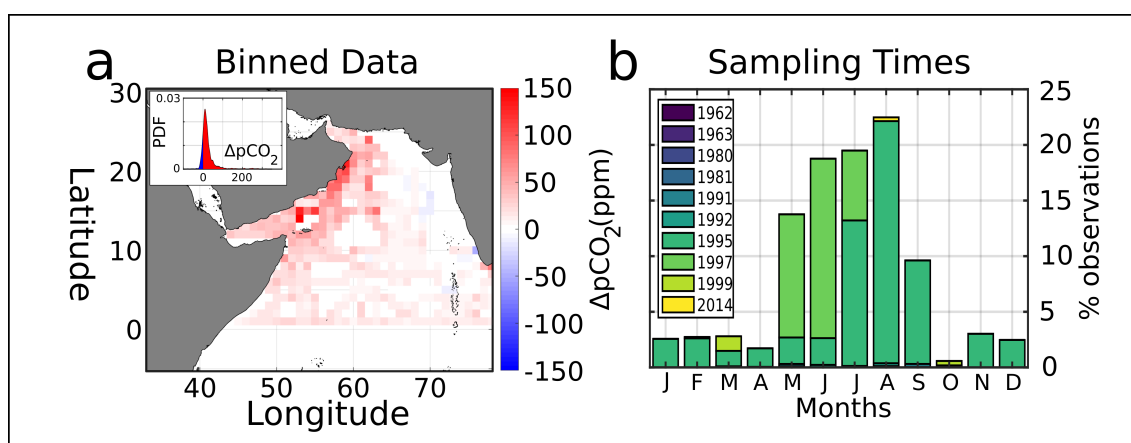
Figure 2. (a) Average surface *in situ* ΔpCO_2 (ppm), with probability density function (PDF) of all ΔpCO_2 values inset. ΔpCO_2 data are calculated in comparison to Keeling atmospheric pCO_2, then binned into a 1^ox1^o grid. (b) Monthly distribution of *in situ* data sampling times, color-coded by sampling year.
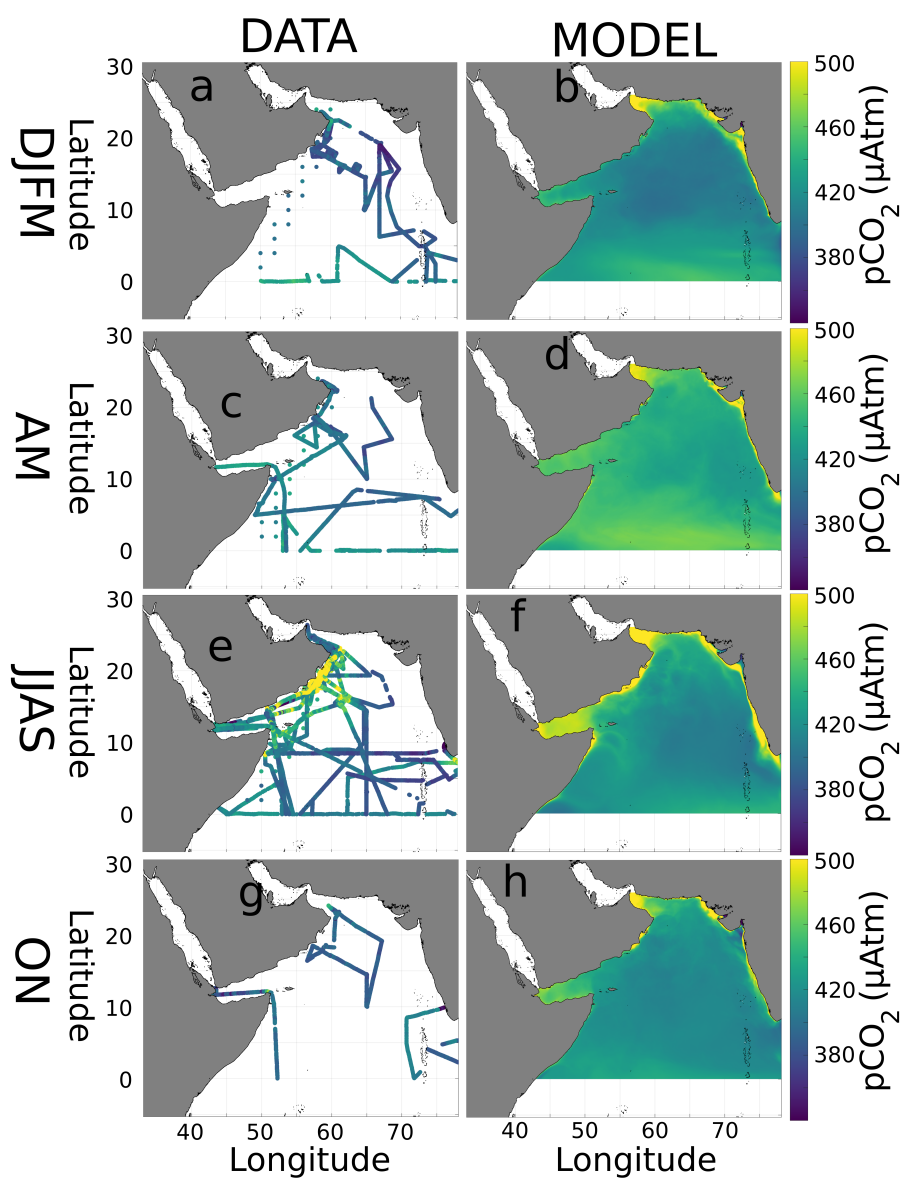
Figure 3. Seasonal surface pCO₂ (µatm) from data (a-d) and the model (e-h), representing winter monsoon DJFM (a,e), spring intermonsoon AM (b,f), summer monsoon JJAS (c,g), and fall intermonsoon ON (d,h).
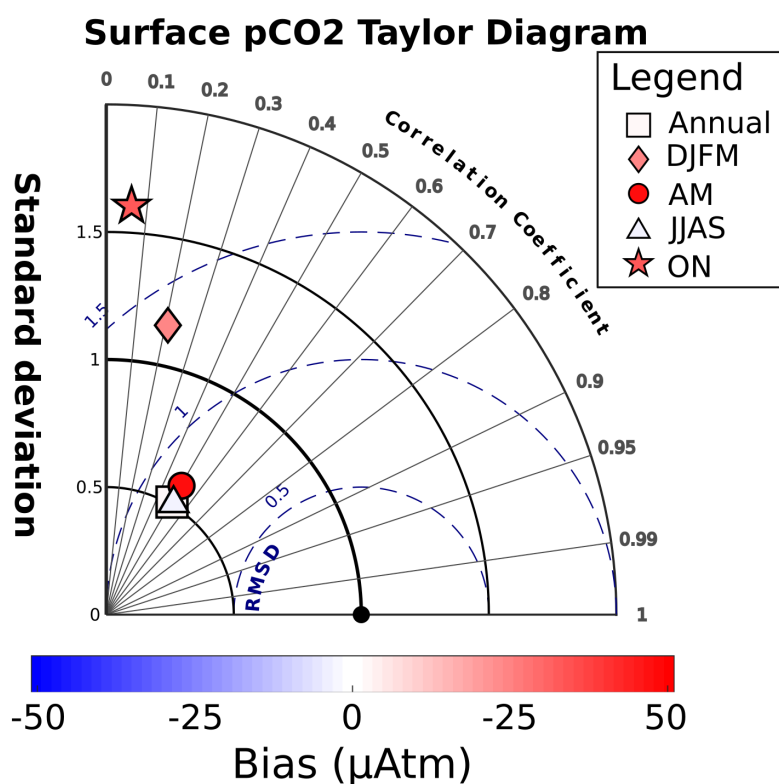
Figure 4. Taylor diagram of modeled vs. observed surface pCO₂, both in total and seasonal sub-sampling. Data are from merged SOCAT and LDEO databases, corrected to year 2005. Distance frmo origin (concentric solid lines) is normalized model standard deviation. Angle from vertical axis is Pearson correlation coefficient. Distance from observation point (black dot) is root-mean square deviation (blue dashed lines). Color of each point denotes model bias, *i.e.* positive values are overestimate.
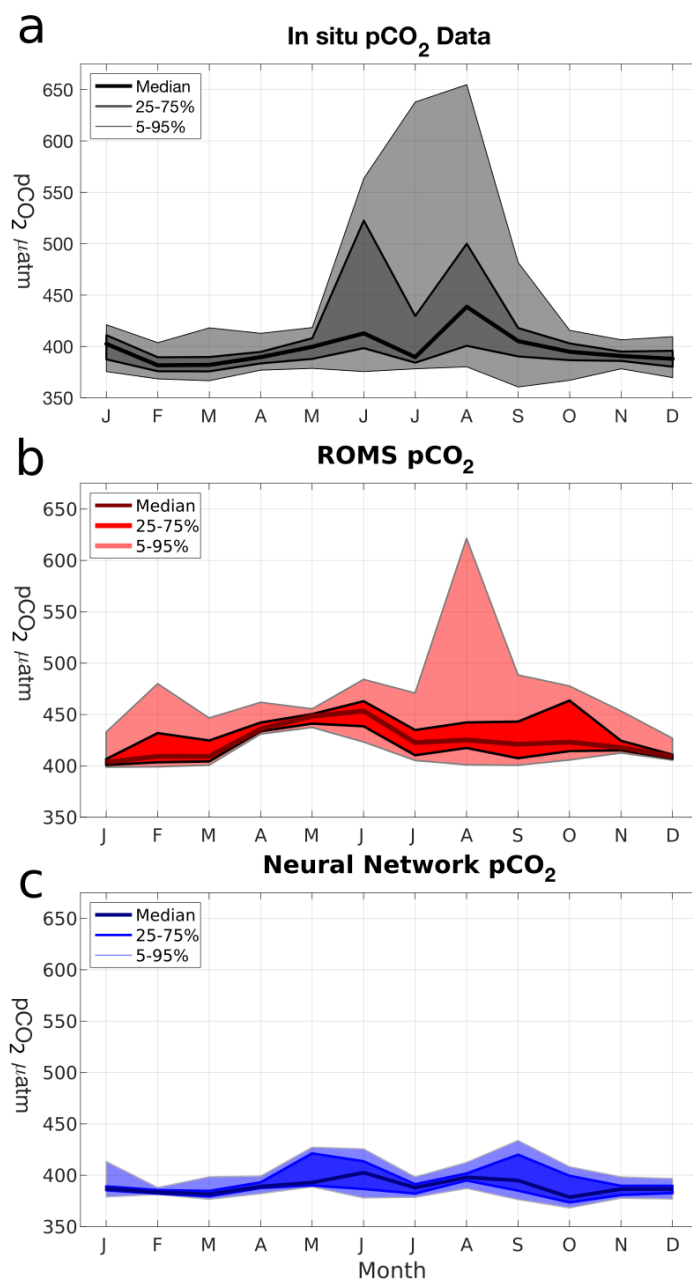
Figure 5. Monthly probability density distributions of surface pCO₂ in (a) merged SOCAT/LDEO *in situ* data, (b) modeled pCO₂, and (c) L15 pCO₂ climatology.
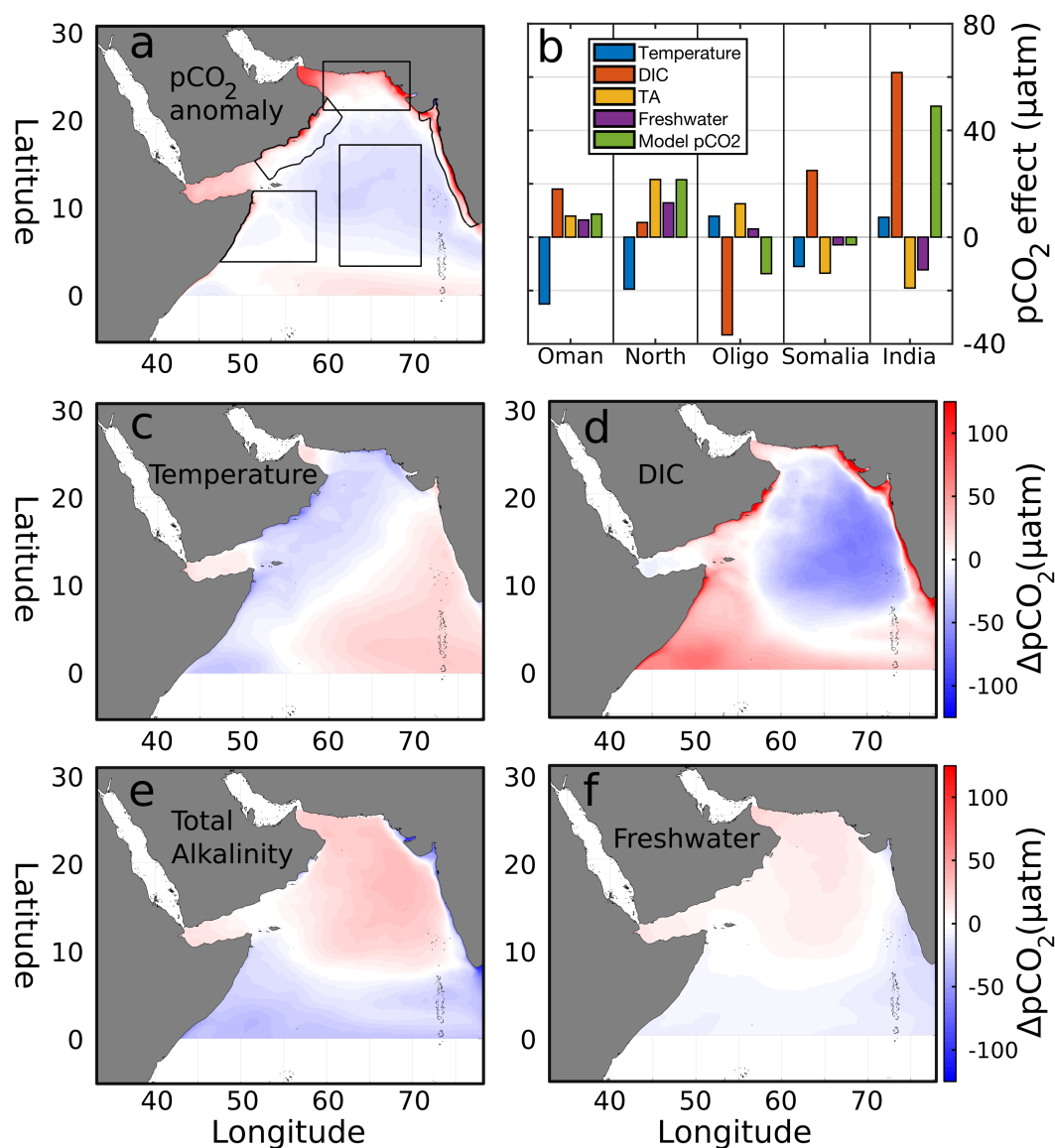
Figure 6. (a) Spatial anomaly of time-averaged surface pCO₂ (μatm). Black boxes represent regions of analysis used in (b) to show averaged contributions of four variables to pCO₂ variability. The changes in pCO₂ due to these variables are shown for (c) temperature, (d) DIC, (e) TA, and (f) freshwater.
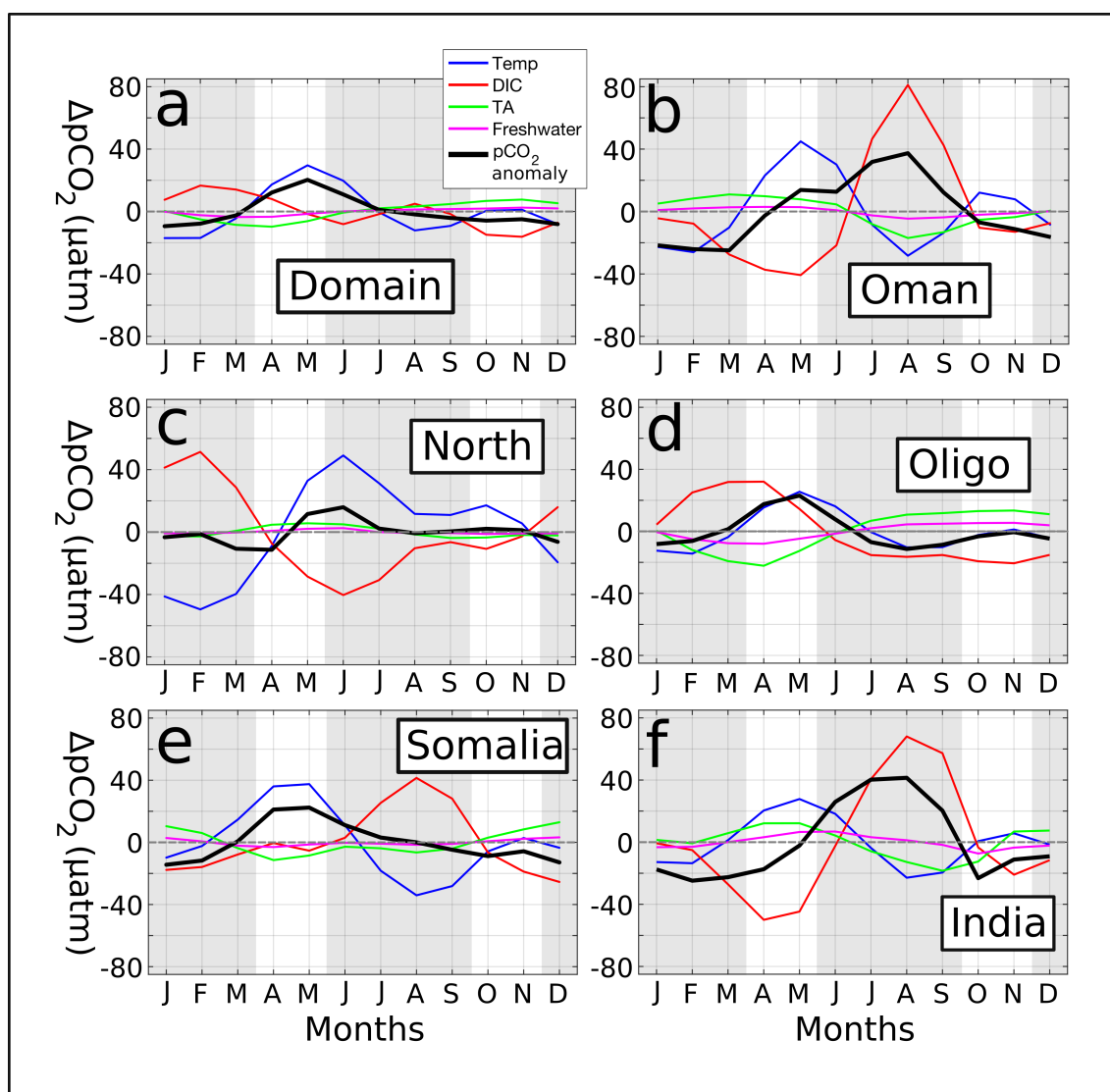
Figure 7. Timeseries of pCO$_2$ anomalies (μatm) (black lines) for (a) the entire domain, (b) Oman, (c) North AS, (d) oligotrophic central AS, (e) Somalia, and (f) India. Dashed gray lines indicates horizontal axis. Gray shading shows summer and winter monsoons. Additional lines show change in pCO$_2$ due to temperature (blue), DIC (red), TA (green), and freshwater (magenta).
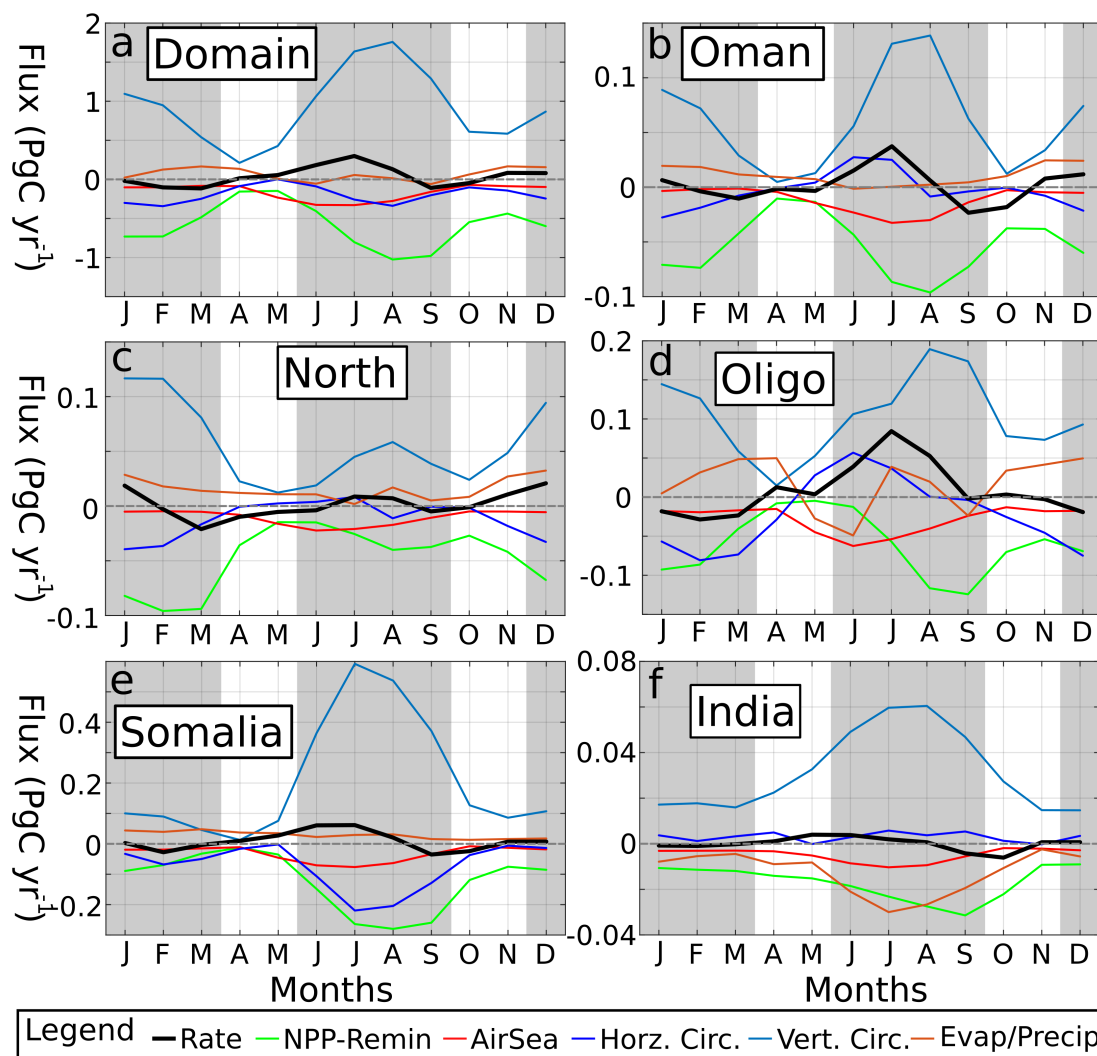
Figure 8. Timeseries of DIC fluxes ($PgCyr^{-1}$) in the top 20 m for (a) the domain, (b) Oman, (c) North AS, (d) oligotrophic central AS, (e) Somalia, and (f) India. Dashed gray line shows x=zero axis. Gray shading denotes summer and winter monsoons, similar to Fig. 8.
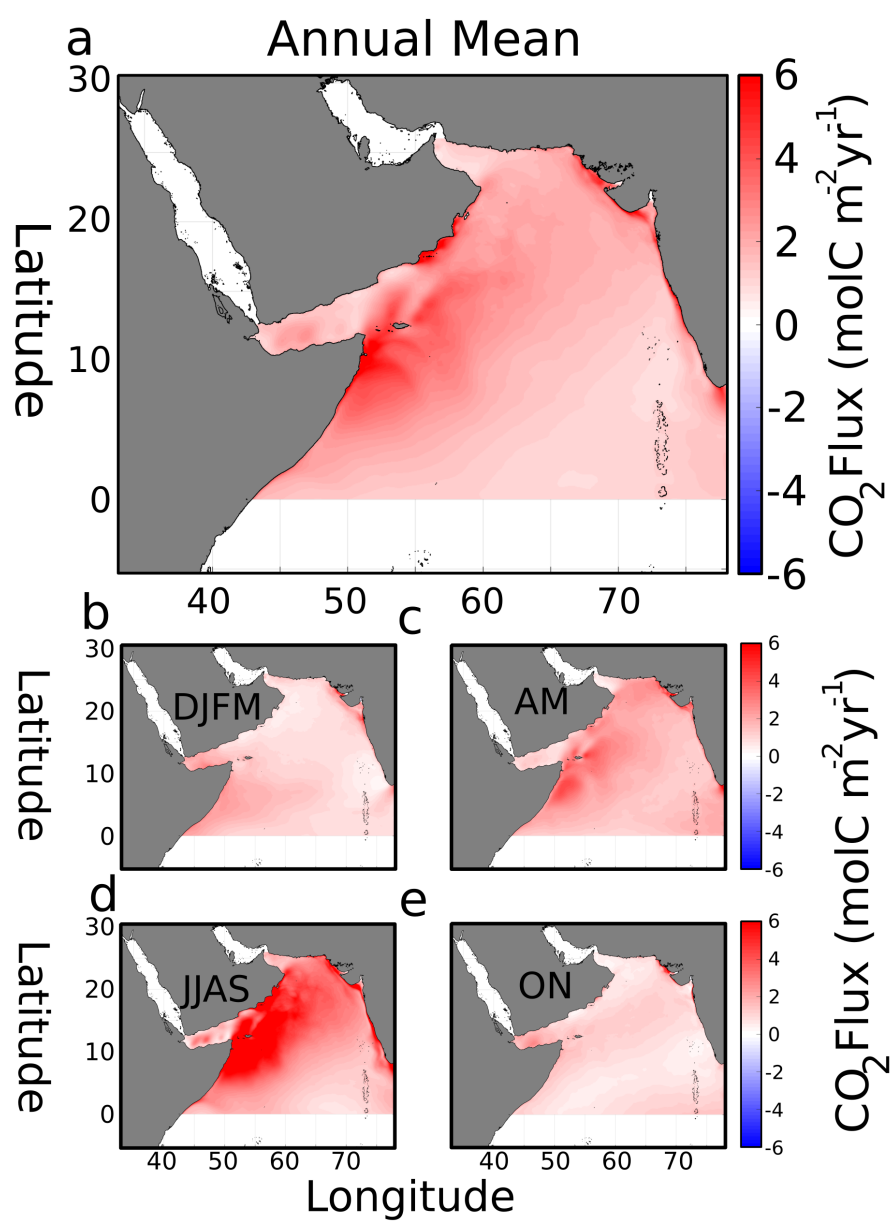
Figure 9. (a) Modeled annual mean air-sea CO_2 flux density $(molCm^{-2}yr^{-1})$. (b-e) Seasonal flux density for winter DJFM, spring AM, summer JJAS, and fall ON, respectively. Positive is flux out of the ocean.
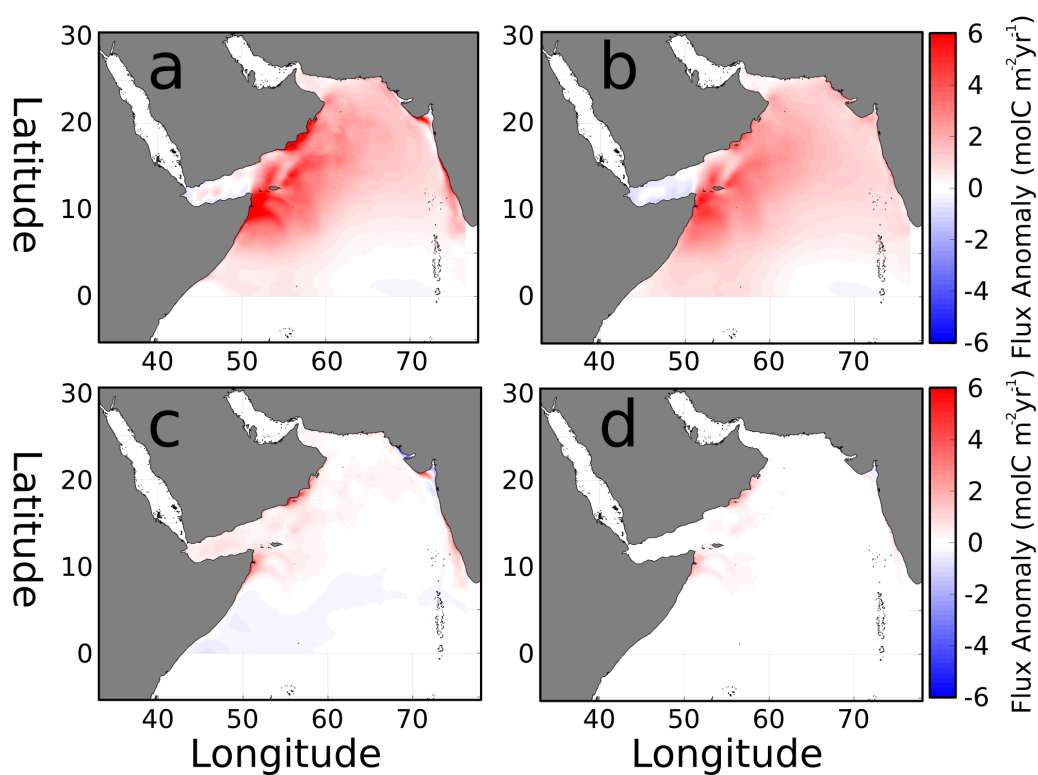
Figure 10. (a) Anomaly of air-sea CO_2 flux during summer monsoon JJAS ($\mathrm{molCm^{-2}yr^{-1}}$. Summer flux anomaly contributions due to (b) wind, (c) pCO_2, and (d) cross-terms in Eqn.(8).
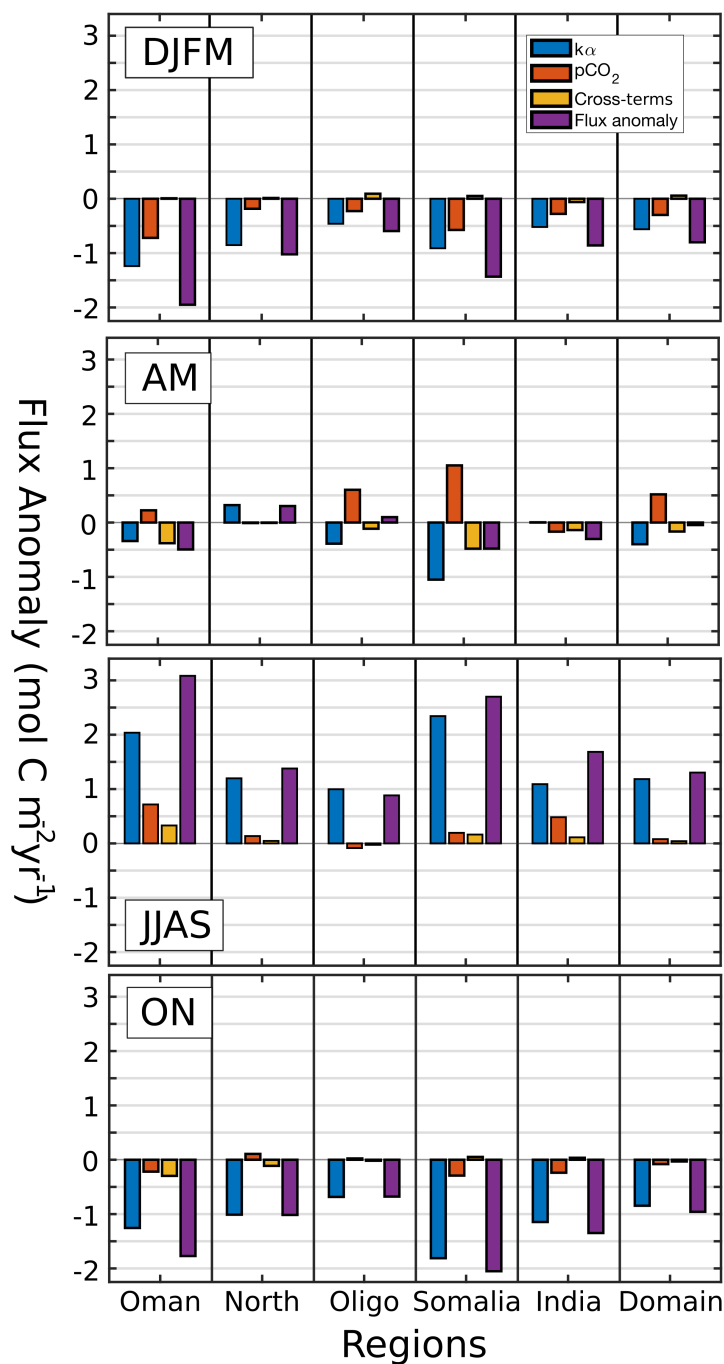
Figure 11. Seasonal CO_2 flux anomaly (purple) for winter DJFM monsoon (top-left), spring AM (top-right), summer monsoon JJAS (bottom-left), and fall ON (bottom-right). Contributors to the flux are solubility/winds ($k\alpha$,blue), pCO_2 (red), and cross-terms (yellow). Results are shown for entire domain and sub-regions.
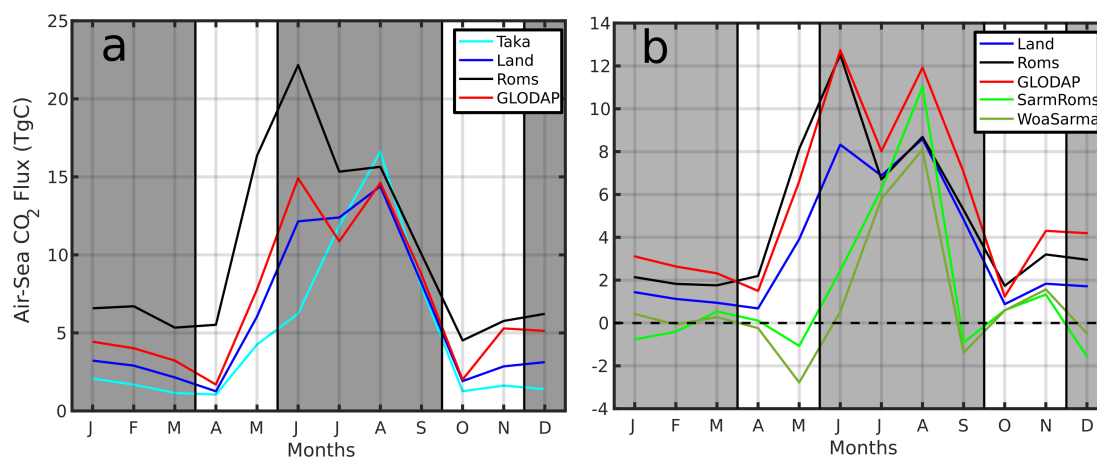
Figure 12. (a) Monthy CO_2 flux (TgC) from the AS as calculated using pCO_2 from TK09 (cyan), L15 (blue), model (black), and GLODAP (red). (b) Monthly CO_2 flux from 10^oN and north using pCO_2 from L15 (blue), model (black), GLODAP (red), Sarma using model output (bright green), and Sarma using WOA data (dark green). Dashed line in (b) is the zero flux axis, gray regions denote winter and summer monsoons. Positive flux is out from the ocean surface.

Table 1. Summary of pCO$_2$ datasets used in this study. Included is whether the product is gridded, and if so, its spatial and temporal resolution. Reference year (Ref. Yr) indicates the year from which Keeling atmospheric xCO$_2$ values are used to calculate CO$_2$ flux. Purpose designates use case within the article. pCO$_2$ calculated indicates whether product provides pCO$_2$ (No) or whether pCO$_2$ was calculated using DIC, TA, temperature, salinity, and possibly Chl-a (Yes).

Dataset	Gridded (Y/N), Resolution	Ref. Year (xCO$_2$)	Domain	Purpose	pCO$_2$ calculated	Reference
Surface Ocean Carbon Atlas (SOCAT)	No, N/A	2005	Global	Model pCO$_2$ validation	No	Bakker et al. (2016)
Lamont-Doherty Earth Observatory pCO$_2$ database (LDEO)	No, N/A	2005	Global	Model pCO$_2$ validation	No	Takahashi et al. (2019)
Takahashi 2009 (TK09)	Yes, 4°x5°, monthly	2005	Global	Air-Sea CO$_2$ flux estimate	No	Takahashi et al. (2009)
Landschützer 2015 (L15)	Yes, 1°x1°, monthly	2001	Global	pCO$_2$ comparison and Air-Sea CO$_2$ flux estimate	No	Landschützer et al. (2015)
Sarma statistical model, T/S/Chl-a from model (ROMS)	Yes, 1/24° (interpolated to 1°), seasonal	1995	AS north of 10°N	Air-Sea CO$_2$ flux estimate	Yes	Sarma (2003)
Sarma statistical model, World Ocean Atlas T/S, SeaWifs Chl-a	Yes, 1°x1°, seasonal	1995	AS north of 10°N	Air-Sea CO$_2$ flux estimate	Yes	Sarma (2003)
GLODAP DIC/TA, World Ocean Atlas T/S	Yes, 1°x1°, annual	2002	Global	Air-Sea CO$_2$ flux estimate	Yes	Olsen et al. (2019)